Fractional Order Stochastic Image Integration Models and Deep Learning of Multi-Fractional Interactions

Abdourrahmane Atto

Fractional Order Stochastic Image Integration Models and Deep Learning of Multi-Fractional Interactions

Abdourrahmane M. ATTO[1]

***Abstract*—The paper provides 3 main contributions for the analysis and simulation of fractionally integrated stochastic image fields. The first two contributions are dedicated to the definition of fields either directly on discrete spatial grids or by referring to continuous spatial frameworks. For the discrete spatial grid framework, the paper proposes a new class of fractionally integrated fields and derives their spectral characterizations, as well as a procedure for stochastic simulation of their samples. Concerning the continuous spatial framework, the paper proposes a stochastic integration framework for providing a sense to some classes of generalized fractional Brownian fields. For both continuous and spatial frameworks, a practical challenge is the determination of model intrinsic dimension in terms of minimum description length. In this respect, the paper addresses the identification of fractional singular frequency points (called poles), that is the number of interacting fractional integral operators, by designing a deep convolutional neural network trained on spectra of simulated multi-fractional textures. Dimensioning these multiple interactions is shown intricate due to the fact that fractionally integrated fields may exhibit infinite variances at several frequency points, leading to almost undistinguishable situations.**

Keywords – Fractional integration, Stochastic fields, Spectral analysis, Texture synthesis, Spectral learning.

I. Introduction

VISUAL information is a concept where the notion of *variation* plays a central role: for both static and dynamic vision systems, perceptual information is associated with edges and changes in optical flow in order to infer shapes of objects (in a single image or a static scene) or scene reconfiguration (in a video or a dynamic vision system). When edges are abundant in a given scene, the observation refers to the notion of *texture* and the scene under consideration is more complex for visual analysis/compression/interpretation due to a large amount of variations to handle. A theory of visual information has to take into consideration, parsimonious descriptions for textures in terms of their descriptions with as few parameters as possible.

The issue addressed in this paper is some contributions in visual information theory by the proposal of a parsimonious framework for synthesizing non-trivial textures: 1) from basic inputs such as white noise samples and 2) when considering fractional integration operating on very few parameters. White noise has, by definition, a flat spectral response whereas natural images exhibit wide spectral variability, specifically in presence of texture. Starting from a white noise, one can build integration procedures so as to constrain the output for presenting shapes, forms and textures that deserve interests in visual perception.

Most relevant integration solutions in terms of deriving rich spectral content and visual texture impact involve stochastic fractional order frameworks [1], [2], [3], [4]. Early works in the 1980s have concerned feature extraction from a one-dimensional fractional Brownian motion model [5], [6], [7]. The 1990s decade has established the foundations of the first spatial extensions in terms of isotropic fractional Brownian fields [8], [9], [10] or estimating a fractal dimension from object and scene observations [11], [12]. In the following decade (2000s), efforts have been concentrated on different issues raised by fractional integral image processing, for instance: synthesis schemes in cases of either isotopic guidelines [13] or anisotropic concerns (limited to a pre-specified elliptical form) [14], but also the highlights and benefits of fractional order modeling for biomedical applications [15], [16], [17]. The 2010s have been ages of:

- optimization of algorithms for simulating [3] and characterizing transformations [18] of the oldest but "consistent" isotropic fractional Brownian field model;
- investigations of different methods for parameter estimation [19], [20], [21];
- spreading out fractional analysis to image processing applications such as feature enhancements [4], [22], [23], [24] and feature extraction for clustering, segmentation or pattern recognition purposes [25], [26],

[1] LISTIC, EA 3703, Université Savoie Mont Blanc - Université Grenoble Alpes, France

Email: *Abdourrahmane.Atto@univ-smb.fr* - Phone: +334 50 09 65 27 - Fax: +334 50 09 65 59

The work was supported by PHOENIX ANR-15-CE23-0012 grant of the French *National Agency of Research*.

[27], [28].

This paper provides 3 types of contributions. First, it proposes new explicit discrete domain fractional integration models that ease deriving structured image content from few parameters. Second, it provides a mathematical sense to a general class of continuous domain integration models introduced in the conference paper [1]. Third, it addresses counting multi-fractional interactions in images from deep learning of integral operator interactions and provides an attractive solution that can handle moderately the *curse of power* observed when non-linearity implies multiple spectral explosions and overlays of mutual spectral grows.

The paper is organized as follows. Section II provides, in a discrete 2D framework, some preliminary results on discrete fractional integration and a new class of multi-fractional parametric forms that makes possible the synthesis of textures with rich visual content. Section III recall some extensions of continuous domain generalized fractional order Brownian fields introduced in [1] and provides a mathematical sense to their definition. Section IV addresses estimation of the number of multi-fractional interactions from a simulated database of order fractional textures. Section concludes the paper. The overall presentation is centered on presenting the specificity of discrete and continuous domain integration models, prior to addressing multi-fractional interaction count.

II. Fractional order stochastic 2D integral fields

In this section, t, s are discrete time variables, $t, s \in \mathbb{N}, \mathbb{Z}, \ldots$. The section starts (Section II-A) with a presentation of the framework described in [29, In French] for discrete domain fractional order image integration before proposing (Section II-B), from this framework, a new class of parametric forms that have their energy concentrated in few spectral frequencies.

A. Discrete domain fractional order spatio-stochastic integration

1) Basics on discrete spatial fractional order integration: An integrated field $\mathbf{X}$ can be seen as combinations of spatial contributions of an elementary field $\mathbf{Z}$ (white noise in general) measured *via* a spatial shift operator B. Discrete domain integrated fields involve sums:

- that depend only on integer powers of B (integer order integrals) or
- may depend on non-integer real values at the power of B (fractional order integrals).

The shifts associated with operator B require computing a sub-pixel measure for the latter case.

In practice, not any sum forms an integrated process: for integration terminology, operator B must be chosen so that $(\mathbb{1} - B)f(t, s)$ behaves approximately as a discrete partial *spatial derivative* of the function $f(t, s)$. The following provides spatial operators B that respect this requirement.

Definition 1 (Gradient shift operators): Operators

$$B_{\text{Grad-V}} : \mathbf{X}(t, s) \longmapsto \mathbf{X}(t-1, s) \tag{1}$$

$$B_{\text{Grad-H}} : \mathbf{X}(t, s) \longmapsto \mathbf{X}(t, s-1) \tag{2}$$

$$B_{\text{Grad-D}} : \mathbf{X}(t, s) \longmapsto \mathbf{X}(t-1, s-1) \tag{3}$$

are associated with Vertical (Grad-V), Horizontal (Grad-H) and Diagonal (Grad-D) gradient components. ■

These gradient based operators apply strict "back-shifts" and one can check that since $B_{\text{Grad-V}}\mathbf{X}(t, s) = \mathbf{X}(t-1, s)$, then $(\mathbb{1} - B_{\text{Grad-V}})f(t, s) = f(t, s) - f(t-1, s)$ is the standard discrete partial derivative of function f with respect to variable t. Note also that

$$\begin{aligned} B^k_{\text{Grad-V}} f(t, s) &= \underbrace{B_{\text{Grad-V}} B_{\text{Grad-V}} \ldots B_{\text{Grad-V}}}_{k \text{ terms}} f(t, s) \\ &= f(t-k, s) \end{aligned}$$

so that shifting to position $t-k$ involves k times composition of the elementary operator $B_{\text{Grad-V}}$.

Because the gradient operators $B_{\text{Grad-V}}$, $B_{\text{Grad-H}}$, $B_{\text{Grad-D}}$ apply back-shifts, they are called causal (their shifting does not involve an $f(t', s')$ with $t' > t$ or $s' > s$). Shift operator B can also be chosen anti-causal or "neither causal, nor anti-causal" with possible neighborhood consideration: for instance, since the standard Laplace operator satisfies:

$$\Delta f = f(t+1, s) + f(t-1, s) + f(t, s+1) + f(t, s-1) - 4f(t, s)$$

then one can derive, by seeking B_{Lap} such that $(1 - B_{\text{Lap}})f(t, s) \propto \Delta f(t, s)$:

Definition 2 (Laplace shift operator): The operator B_{Lap} defined by:

$$\begin{aligned} B_{\text{Lap}}\mathbf{X}(t, s) = \frac{1}{4}\Big(&\mathbf{X}(t+1, s) + \mathbf{X}(t-1, s) \\ &+ \mathbf{X}(t, s+1) + \mathbf{X}(t, s-1)\Big) \end{aligned} \tag{4}$$

is called *Laplace shift operator*. ■

The Laplace shift operator B_{Lap} is a combination that applies on the 4 closest variables pertaining to the neighborhood of $\mathbf{X}(t, s)$, without taking the latter into consideration. The following shift operators called Canny and Prewitt are compositions including the random variable $\mathbf{X}(t, s)$ and are neither causal, nor anti-causal.

Definition 3 (Canny shift operators): Canny Vertical (Can-V) and Horizontal (Can-H) shift operators are defined by:

$$\begin{aligned} B_{\text{Can-V}} : \mathbf{X}(t, s) \longmapsto &\mathbf{X}(t, s) + \mathbf{X}(t-1, s) \\ &- \mathbf{X}(t+1, s) \end{aligned} \tag{5}$$

$$B_{\text{Can-H}} : \mathbf{X}(t,s) \longmapsto \mathbf{X}(t,s) + \mathbf{X}(t,s-1) - \mathbf{X}(t,s+1) \quad (6)$$

■

Definition 4 (Prewitt shift operators): Prewitt Vertical (Pre-V) and Horizontal (Pre-H) shifts consist in:

$$B_{\text{Pre-V}}\mathbf{X}(t,s) = \mathbf{X}(t,s) + \sum_{k=-1}^{1} \mathbf{X}(t-1,s-k) - \sum_{k=-1}^{1} \mathbf{X}(t+1,s-k) \quad (7)$$

and

$$B_{\text{Pre-H}}\mathbf{X}(t,s) = \mathbf{X}(t,s) + \sum_{k=-1}^{1} \mathbf{X}(t-k,s-1) - \sum_{k=-1}^{1} \mathbf{X}(t-k,s+1) \quad (8)$$

■

Remark 1 (From derivation to integration): For $B = B_{\text{Grad-V}}$ defined by Eq. (1), we have seen that $(1 - B_{\text{Grad-V}})f(t,s) = f(t,s) - f(t-1,s)$ is a discrete partial derivative. When considering the inverse (thus integral) operator $(1 - B_{\text{Grad-V}})^{-1}$, we obtain, provided that function g used below is chosen so that the following sum exists:

$$(1 - B_{\text{Grad-V}})^{-1} g(t,s) = \sum_{k \geqslant 0} B^k_{\text{Grad-V}} g(t,s) = \sum_{k \geqslant 0} g(t-k,s)$$

■

Remark 1 above illustrates that one can switch from partial derivation induced by the difference operator $(1 - B)$ to partial integration by inverting the latter and this, for any of the shift operators given by Eqs. (1), (2), (3), (4), (5), (6), (7) and (8).

More generally, we can consider a derivation scheme represented by a function of operator, say $G(B)$, and equations having the form $G(B)f(t,s) = h(t,s)$. The following properties then holds true: if $G(B)$ is a derivation operator, then f is an integral of h and *vice versa*. Note that $G(B)$ can operate integer or fractional order derivation, for instance:

- $(1 - B_{\text{Grad-V}})f$ [from integer power "1" at the power of $(1 - B_{\text{Grad-V}})$] is the integer order derivation of f whereas
- $(1 - B_{\text{Grad-V}})^{1/2} f$ is the fractional order "1/2" derivation of f with respect to B.

Finally, when h is the solution of $(1 - B_{\text{Grad-V}})^{\lambda} f = h$ where $0 < \lambda < 1$, then f is said to be associated with a fractional order λ integral of h.

2) Fractional order spatio-stochastic K-factor Gegenbauer series: In the following, we consider equations with the form $G(B)\mathbf{X}(t,s) = \mathbf{Z}(t,s)$ where $\mathbf{X}, \mathbf{Z} : \mathbb{N} \times \mathbb{N} \times \Omega \longrightarrow \mathbb{R}$ are random fields and $G(B)$ behaves as a fractional order derivation operator (see Section II-A1). Field $\mathbf{X}$ will be said fractional integral of $\mathbf{Z}$.

Definition 5 (K-factor Gegenbauer field): Field $\mathbf{X}(t,s)$ will be called spatial (2D) K-factor B-Gegenbauer (K−B−G) field if it satisfies:

$$\prod_{k=1}^{K} \left(\mathbb{1} - 2\nu_k B + B^2\right)^{b_k} \mathbf{X}(t,s) = \mathbf{Z}(t,s) \quad (9)$$

where $|\nu_k| \leqslant 1$ for any $k = 1, 2, \ldots, K$ and $\mathbf{Z}(t,s)$ is assumed to be a zero-mean white Gaussian field. ■

In Eq. (9), a term $\left(\mathbb{1} - 2\nu B + B^2\right)^b$ behaves as $(\mathbb{1} - B)^{2b}$ when ν is close to 1. Hence K-factor Gegenbauer fields include standard fractionally integrated fields especially when one among the $\nu_k, k = 1, 2, \ldots, K$ is close to one. Assuming a revertible power series expansion of any $\left(\mathbb{1} - 2\nu_k B + B^2\right)^{b_k}$, synthesis of a K-factor Gegenbauer involves computing:

$$\mathbf{X}(t,s) = \prod_{k=1}^{K} \left(\mathbb{1} - 2\nu_k B + B^2\right)^{-b_k} \mathbf{Z}(t,s) \quad (10)$$

where:

$$\left(\mathbb{1} - 2\nu_k B + B^2\right)^{-b_k} = \sum_{\ell=0}^{+\infty} \binom{b_k}{\ell}^{\dagger} (\nu_k)\ B^{\ell} \quad (11)$$

and the Gegenbauer function $\binom{b_k}{\ell}^{\dagger}(\bullet)$ being:

$$\binom{b_k}{\ell}^{\dagger}(x) = \sum_{m=0}^{\lfloor \ell/2 \rfloor} (2x)^{\ell - 2m} \frac{(-1)^m \Gamma(b_k + \ell - m)}{m!\,(\ell - 2m)!\,\Gamma(b_k)} \quad (12)$$

with $\lfloor\rfloor$ denoting the floor function ($\lfloor z \rfloor$ is the largest integer less than or equal to z) and the *Gamma* function is defined by:

$$\Gamma(x) = \int_{\mathbb{R}^+} u^{x-1} e^{-u} du \quad (13)$$

Samples of K-factor B-Gegenbauer fields are given by Figure 1 when B is one among the operators defined by Eqs. (4), (5), (6), (7) and (8). Depending on the operator used, one can obtain either a stochastic texture without any privileged orientation (case of B-Gegenbauer) or textures associated with a main Vertical/Horizontal/Diagonal edge orientation. Note that white noise shows no edge and the texture properties is driven by the operator B selected. More precisely, these texture feature orientations can be inferred from the spectral properties of K-factor B-Gegenbauer fields given below.

***Proposition** 1 (Power Spectral Densities, PSD, of K−B−G fields [29]):* The PSD associated with K-factor B-Gegenbauer fields are given below (PSD notation γ_{K-B-G}

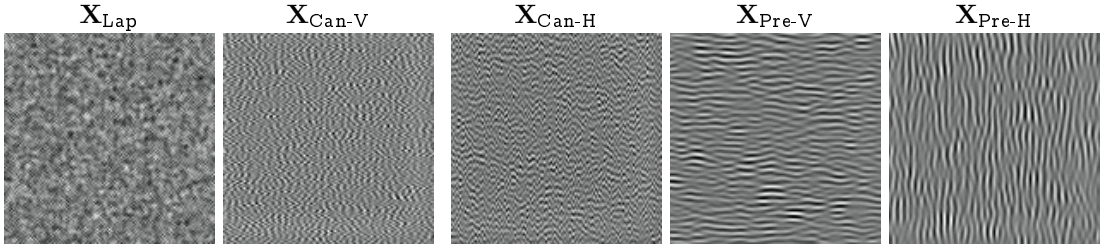

Fig. 1. *5-factor Gegenbauer (see Eq.* (9)*) Laplacien (see Eqs. 4), Canny (see Eqs.* (5) *and* (6)*) and Prewitt (see Eqs.* (7) *and* (8)*).*

for field notation $\mathbf{X}_{K-B-G}$) respectively for the gradient, Laplace, Canny and Prewitt operators, where $\theta_k = 1+\nu_k$ and $\xi_k = 1-\nu_k$.

(i) PSD of $\mathbf{X}_{K-B-G}$ for gradient shift operators (see Eqs. (1), (2), (3), respectively):

$$\gamma_{K-B_{\text{Grad-V}}-G}(\omega_1,\omega_2) = \frac{\sigma^2 \prod_{k=1}^{K} 2^{-2b_k}}{\prod_{k=1}^{K} |\cos\omega_1 - \nu_k|^{2b_k}} \quad (14)$$

$$\gamma_{K-B_{\text{Grad-H}}-G}(\omega_1,\omega_2) = \frac{\sigma^2 \prod_{k=1}^{K} 2^{-2b_k}}{\prod_{k=1}^{K} |\cos\omega_2 - \nu_k|^{2b_k}} \quad (15)$$

$$\gamma_{K-B_{\text{Grad-D}}-G}(\omega_1,\omega_2) = \frac{\sigma^2 \prod_{k=1}^{K} 2^{-2b_k}}{\prod_{k=1}^{K} |\cos(\omega_1+\omega_2) - \nu_k|^{2b_k}} \quad (16)$$

(ii) PSD of $\mathbf{X}_{K-B-G}$ for Laplace shift operator (see Eq. (4)):

$$\gamma_{K-B_{\text{Lap}}-G}(\omega_1,\omega_2) = \frac{\sigma^2}{\prod_{k=1}^{K} \left| \left(\cos^2\left(\frac{\omega_1}{2}\right) + \cos^2\left(\frac{\omega_2}{2}\right) - \theta_k\right)^2 + \theta_k\xi_k \right|^{2b_k}} \quad (17)$$

(iii) PSD of $\mathbf{X}_{K-B-G}$ for Canny shift operators (see Eqs. (18), (19), respectively):

$$\gamma_{K-B_{\text{Can-V}}-G}(\omega_1,\omega_2) = \frac{\sigma^2 \prod_{k=1}^{K} 2^{-2b_k}}{\prod_{k=1}^{K} \left| 4\sin^4\omega_1 - 4\nu_k\xi_k\sin^2\omega_1 + \xi_k^2 \right|^{b_k}} \quad (18)$$

$$\gamma_{K-B_{\text{Can-H}}-G}(\omega_1,\omega_2) = \frac{\sigma^2 \prod_{k=1}^{K} 2^{-2b_k}}{\prod_{k=1}^{K} \left| 4\sin^4\omega_2 - 4\nu_k\xi_k\sin^2\omega_2 + \xi_k^2 \right|^{b_k}} \quad (19)$$

(iv) PSD of $\mathbf{X}_{K-B-G}$ for Prewitt shift operators (see Eqs. (20) and (21), respectively):

$$\gamma_{K-B_{\text{Pre-V}}-G}(\omega_1,\omega_2) = \frac{\sigma^2 \prod_{k=1}^{K} 2^{-2b_k}}{\prod_{k=1}^{K} \left| 4(1+2\cos\omega_2)^2\sin^2\omega_1 - \xi_k^2 \right|^{2b_k}} \quad (20)$$

$$\gamma_{K-B_{\text{Pre-H}}-G}(\omega_1,\omega_2) = \frac{\sigma^2 \prod_{k=1}^{K} 2^{-2b_k}}{\prod_{k=1}^{K} \left| 4(1+2\cos\omega_1)^2\sin^2\omega_2 - \xi_k^2 \right|^{2b_k}} \quad (21)$$

■

Directed vertical, horizontal or diagonal edges occur when a given PSD has its energy concentrated on certain frequency bands or varies only across one single variable (case for gradient and Canny operators). In particular, gradient fields exhibit an infinite number of poles along many axes but in the same direction towards:

- frequencies
$$\{(\omega_1,\omega_2) \in \mathbb{R}^2 / \omega_1 = \text{acos}(\nu_k), k = 1,2,\ldots,K\}$$
for field $\mathbf{X}_{K-B_{\text{Grad-V}}-G}$,
- frequencies
$$\{(\omega_1,\omega_2) \in \mathbb{R}^2 / \omega_2 = \text{acos}(\nu_k), k = 1,2,\ldots,K\}$$
for field $\mathbf{X}_{K-B_{\text{Grad-H}}-G}$ and
- frequencies
$$\{(\omega_1,\omega_2) \in \mathbb{R}^2 / \omega_1+\omega_2 = \text{acos}(\nu_k), k = 1,\ldots,K\}$$
for field $\mathbf{X}_{K-B_{\text{Grad-D}}-G}$.

K-factor Canny-Gegenbauer fields present strong similarities with their analog gradient fields by construction, but they admit no pole when $|\nu_k| < 1$ for any k.

From Proposition 1, only Laplace and Prewitt fields show more complex PSD. However, K-factor Laplace-Gegenbauer fields $\mathbf{X}_{K-B_{\text{Lap}}-G}$ have no pole (dominant frequency) when the absolute value of every ν_k is < 1 and are isotropic up to the mapping: $\omega_i \mapsto \cos(\omega_i/2)$ (same property whatever the direction). The motivation of the following section is the proposal of spatial field models with richer PSD content in terms of spectral variability as well as limiting the number of poles.

B. Fractionally integrated fields from double indexed Gegenbauer polynomials

For being able to generate textures with parsimonious spectral information, we need to control PSD behavior in specific frequencies of interest. This cannot be achieved straightforwardly when using Definition II-A2. To overcome this limitation, the main contribution of this section is the construction of double indexed spatial multifractional integral models.

Definition 6 (K-factor doubly indexed Gegenbauer field):

Field $\mathbf{X}(t,s)$ will be called K-factor Doubly Indexed Gegenbauer (K-DI-G) field if it satisfies one of the equations given below:

$$\prod_{k=1}^{K}\Big(\epsilon_1 B_1^{-2}\left(\mathbb{1}-2\mu_k B_1+B_1^2\right)^2+ \epsilon_2 B_2^{-2}\left(\mathbb{1}-2\nu_k B_2+B_2^2\right)^2\Big)^{b_k}\mathbf{X}(t,s)=\mathbf{Z}(t,s) \quad (22)$$

or

$$\prod_{k=1}^{K}\Big(\epsilon_1 B_2^{2}\left(\mathbb{1}-2\mu_k B_1+B_1^2\right)^2+ \epsilon_2 B_1^{2}\left(\mathbb{1}-2\nu_k B_2+B_2^2\right)^2\Big)^{b_k}\mathbf{X}(t,s)=\mathbf{Z}(t,s) \quad (23)$$

where $|\mu_k|\leqslant 1$ and $|\nu_k|\leqslant 1$ for any $k=1,2,\ldots,K$; B_1 and B_2 are spatial shift operators chosen conveniently; $\mathbf{Z}(t,s)$ is a zero-mean white Gaussian noise and ϵ_1,ϵ_2 are positive real valued parameters. ■

Eqs. (22) and (23) show a balance between two Gegenbauer polynomials, the balance being governed by parameters ϵ_1 and ϵ_2. When B_1 and B_2 are causal operators (gradient operators for instance), then Eq. (22) presents backward and forward shifts whereas Eq. (23) highlights only backward shifts.

Synthesis of sample $\mathbf{X}(t,s)$ satisfying Eq. (22) requires computing:

$$\mathbf{X}(t,s)=\prod_{k=1}^{K}\Big(\epsilon_1 B_1^{-2}\left(\mathbb{1}-2\mu_k B_1+B_1^2\right)^2+ \epsilon_2 B_2^{-2}\left(\mathbb{1}-2\nu_k B_2+B_2^2\right)^2\Big)^{-b_k}\mathbf{Z}(t,s) \quad (24)$$

thus, decomposing the fractional double indexed polynomial as series involving integer powers of B_1 and B_2 (field $\mathbf{Z}(t,s)$ is available only for $t,s\in\mathbb{Z}$ in the discrete domain framework). For this purpose, we write:

$$\mathbf{X}(t,s)=\prod_{k=1}^{K}\left(\epsilon_1\left(\frac{B_1^{-1}+B_1}{2}-\mu_k\right)^2+ \epsilon_2\left(\frac{B_2^{-1}+B_2}{2}-\nu_k\right)^2\right)^{-b_k}\mathbf{Z}(t,s) \quad (25)$$

and set, for $i=1,2$,

$$\overline{B}_i=\sqrt{\epsilon_i}(B_i^{-1}+B_i)/2 \quad (26)$$

In this respect, we are concerned by:

$$\mathbf{X}(t,s)=\prod_{k=1}^{K}\Big(\left(\overline{B}_1-\sqrt{\epsilon_1}\mu_k\right)^2 + \left(\overline{B}_2-\sqrt{\epsilon_2}\nu_k\right)^2\Big)^{-b_k}\mathbf{Z}(t,s) \quad (27)$$

which amounts, by noting $\overline{\mu}_k=\sqrt{\epsilon_1}\mu_k$, $\overline{\nu}_k=\sqrt{\epsilon_2}\nu_k$ and $c_k=\overline{\mu}_k^2+\overline{\nu}_k^2$, to:

$$\mathbf{X}(t,s)=\prod_{k=1}^{K}\Big(c_k-2\overline{\mu}_k\overline{B}_1 - 2\overline{\nu}_k\overline{B}_2+\overline{B}_1^2+\overline{B}_2^2\Big)^{-b_k}\mathbf{Z}(t,s) \quad (28)$$

The latter is an extension of the Gegenbauer polynomial introduced in [30, Eqs. (1) and (18)].

Denote, for $k=1,2,\ldots,K$,

$$\mathbf{X}_k(t,s)=\Big(c_k-2\overline{\mu}_k\overline{B}_1 - 2\overline{\nu}_k\overline{B}_2+\overline{B}_1^2+\overline{B}_2^2\Big)^{-b_k}\mathbf{X}_{k-1}(t,s) \quad (29)$$

with the convention $\mathbf{X}_0=\mathbf{Z}$. The recursive Eq. (29) implies $\mathbf{X}_K=\mathbf{X}$ and we have:

Proposition 2: $\mathbf{X}_k(t,s)=\lim_{M,N\to+\infty}\mathbf{X}_{k,M,N}(t,s)$ with

$$\mathbf{X}_{k,M,N}(t,s)=\sum_{m,n=0}^{M}C_{m,n}^{b_k}(\overline{\mu}_k,\overline{\nu}_k)\overline{B}_1^m\overline{B}_2^n\mathbf{X}_{k-1}(t,s) \quad (30)$$

where function $C_{m,n}^{b}$ is defined by:

$$C_{m,n}^{b}(\mu,\nu)=\sum_{p=0}^{\lfloor m/2\rfloor}\sum_{q=0}^{\lfloor n/2\rfloor}\frac{(-1)^{p+q}\Gamma(b+m+n-p-q)}{\Gamma(b)p!\;\;q!\;\;(m-2p)!\;\;(n-2q)!} \times\frac{(2\mu)^{m-2p}(2\nu)^{n-2q}}{c^{m+n-p-q+b}} \quad (31)$$

and the *Gamma* function is given by Eq. (13). ■

Proof: See Appendix A. ■

At this stage, we should specify $\overline{B}_1$ and $\overline{B}_2$ in Eq. (30) before continuing. When $B_1=B_{\text{Grad-V}}^{r_1}$ and $B_2=B_{\text{Grad-H}}^{r_1}$, we have from Eq. (26),

$$\overline{B}_1\overline{B}_2\mathbf{Y}(t,s)=\sqrt{\epsilon_2}\overline{B}_1\left(\frac{\mathbf{Y}(t,s-r_2)+\mathbf{Y}(t,s+r_2)}{2}\right)$$

thus:

$$\overline{B}_1\overline{B}_2\mathbf{Y}(t,s)= \frac{\sqrt{\epsilon_1}\sqrt{\epsilon_2}}{4}\Big(\mathbf{Y}(t-r_1,s-r_2)+\mathbf{Y}(t+r_1,s-r_2) +\mathbf{Y}(t-r_1,s+r_2)+\mathbf{Y}(t+r_1,s+r_2)\Big)$$

In practice, computing $\overline{B}_1^m \overline{B}_2^n \mathbf{Y}(t,s)$ consists in ℓ recursive applications of operator $\overline{B}_1\overline{B}_2$ followed by either $m-\ell$ compositions with $\overline{B}_1$ or $n-\ell$ applications of $\overline{B}_1$, where $\ell = \min\{m,n\}$. Textures given in Figure 2 have been obtained by using $r_1 = r_2 = 1$.

Figure 2 highlights that the doubly indexed polynomials of Eq. (22) yield a more powerful texture synthesis framework than the single one given by Eq. (9). In order to give a more formal proof of the latter assertion, let us derive the PSD associated with K-DI-G. We have:

Proposition 3: For $B_1 = B_{\text{Grad-V}}^{r_1}$ and $B_2 = B_{\text{Grad-H}}^{r_1}$, the PSD associated with a K-DI-G given by either Eq. (22) or (23) is:

$$\gamma(\omega_1,\omega_2) = \frac{\sigma^2 \prod_{k=1}^{K} 2^{-2b_k}}{\prod_{k=1}^{K}\Big(\epsilon_1\left(\cos(r_1\omega_1)-\mu_k\right)^2+\epsilon_2\left(\cos(r_2\omega_2)-\nu_k\right)^2\Big)^{b_k}} \quad (32)$$

Proof: The proof follows from straightforward computations, by taking the moduli of Eqs. (22), (23) and by replacing in these quantities, B_ℓ by $e^{ir_\ell\omega_\ell}$ for $\ell = 1,2$. ∎

The PSD of Eq. (32) shows poles at frequencies $(\omega_1,\omega_2) = \left(\frac{a\cos\mu_k}{r_1}, \frac{a\cos\nu_k}{r_2}\right)$ for $k = 1,2,\ldots,K$. Thus, we can specify specific frequency points associated with energy concentration, which makes K-DI-G a more concise framework for the synthesis of textures with multiple orientated features.

III. Continuous spatial domain fractional order integration models

In this section, t,s are continuous time variables, $t,s \in \mathbb{R}_+, \mathbb{R}, \ldots$ and $\mathbf{X} : (t,s) \mapsto \mathbf{X}(t,s) = \mathbf{X}_\omega(t,s) = \mathbf{X}_{t,s}(\omega) \in \mathbb{R}$ or $\mathbb{C}$ is a spatial stochastic field assumed to be centered in what follows. We recall that a stochastic field $\mathbf{X} = (\mathbf{X}(\bullet,\bullet))$ is Gaussian if the random variable $\mathbf{X}(t,s)$ is Gaussian for every couple (t,s) pertaining to the domain of interest. Assuming that $\mathbf{X}$ is Gaussian, we can focus on its second-order statistics and since $\mathbf{X}$ has been assumed centered, then this field is entirely characterized by its autocorrelation function. Thus, for synthesizing sample realizations of $\mathbf{X}$, we only need to know the analytic form of this autocorrelation function.

As in previous section (dedicated to discrete domain models), the aim addressed in reference [1] was the derivation of a continuous domain fractional field framework associated with parsimonious spectral contents. This aim has led [1] to propose a class of generalized fractional Brownian fields, the generalization concerning a model with 1) an arbitrary number of Hurst parameters and 2) an arbitrary number of spectral singularity points. However, the mathematical sense of these generalized fractional Brownian fields remains unspecified at present time. This section proposes a sense to these fields as a main contribution.

Section recalls the construction that has led to generalize fractional Brownian fields and Section shows that the convolution involved in their construction converges in quadratic mean sense.

A. Generalized Fractional Brownian Fields (GFBF)

GFBF are associated to spatial domain convolution and modulation operators over a sequence of Fractional Brownian Fields (FBF). Process $\mathbf{G}_{\mathcal{H},(u_0,v_0)}$ is called *Modulated Fractional Brownian Field* (MFBF) if it can be written in the form:

$$\mathbf{G}_{\mathcal{H},(u_0,v_0)}(x_1,x_2) = e^{iu_0x_1}e^{iv_0x_2}\mathbf{F}_{\mathcal{H}}(x_1,x_2) \quad (33)$$

where $\mathbf{F}_{\mathcal{H}}$ is a centered isotropic FBF with autocorrelation

$$R_{\mathbf{F}_{\mathcal{H}}}(x_1,x_2,y_1,y_2) = \frac{\sigma^2}{2}\Big((x_1^2+x_2^2)^{\mathcal{H}} + (y_1^2+y_2^2)^{\mathcal{H}} - \left[(x_1-y_1)^2+(x_2-y_2)^2\right]^{\mathcal{H}}\Big) \quad (34)$$

Field $\mathbf{G}_{\mathcal{H},(u_0,v_0)}$ is complex valued and results as the interaction between a stochastic FBF (see first row of Figure 3) and a deterministic phase term (see second row of Figure 3). Field $\mathbf{G}_{\mathcal{H},(u_0,v_0)}$ is centered and its autocorrelation

$$R_{\mathbf{G}_{\mathcal{H},(u,v)}}(x_1,x_2,y_1,y_2) = \mathbb{E}[\mathbf{G}_{\mathcal{H},(u,v)}(x_1,x_2)\,\overline{\mathbf{G}_{\mathcal{H},(u,v)}(y_1,y_2)}] \quad (35)$$

simplifies as

$$R_{\mathbf{G}_{\mathcal{H},(u_0,v_0)}}(x_1,x_2,y_1,y_2) = R_{\mathbf{F}_{\mathcal{H}}}(x_1,x_2,y_1,y_2)e^{iu_0(x_1-y_1)}e^{iv_0(x_2-y_2)} \quad (36)$$

where $R_{\mathbf{F}_{\mathcal{H}}}(x_1,x_2,y_1,y_2)$ is given by Eq. (34). Thus,

$$R_{\mathbf{G}_{\mathcal{H},(u,v)}}(x_1,x_2,y_1,y_2) = \frac{\sigma^2}{2}e^{iu(x_1-y_1)}e^{iv(x_2-y_2)}\Big((x_1^2+x_2^2)^{\mathcal{H}} + (y_1^2+y_2^2)^{\mathcal{H}} - \left[(x_1-y_1)^2+(x_2-y_2)^2\right]^{\mathcal{H}}\Big) \quad (37)$$

The GFBF is an integral representation involving interactions of several MIFBF: consider two sequences, the first

$$\mathfrak{H}_Q = \{\mathcal{H}_1,\mathcal{H}_2,\ldots,\mathcal{H}_Q\}$$

composed of Hurst parameters and the second

$$\{(u_1,v_1),(u_2,v_2),\ldots,(u_Q,v_Q)\}$$

associated with modulation parameters (poles) of Q independant MIFBF $\left(\mathbf{G}_{\mathcal{H}_s,(u_s,v_s)}\right)_{s=1,2,\ldots,Q}$ having autocorrelations: $\left(R_{\mathbf{G}_{\mathcal{H}_s,(u_s,v_s)}}\right)_{s=1,2,\ldots,Q}$. A GFBF $\mathcal{E}_{\mathfrak{H}_Q}$ has

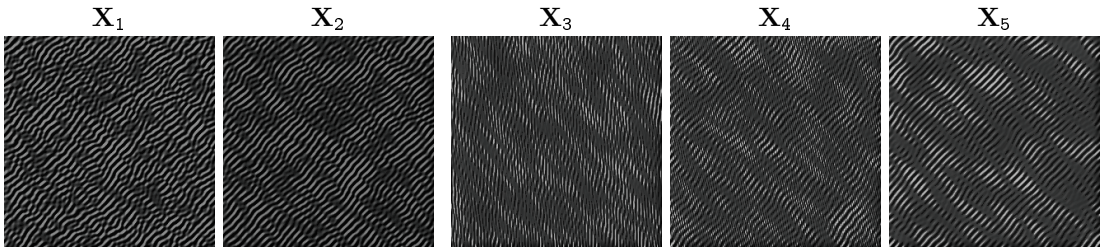

Fig. 2. 1 *to* 5*-DI-G fields generated from random selection of* μ_k, ν_k *by using Eq.* (30) *with* $B_1 = B_{Grad\text{-}V}$ *and* $B_2 = B_{Grad\text{-}H}$ *defined by Eq.* (1) *and* (2) *respectively.*

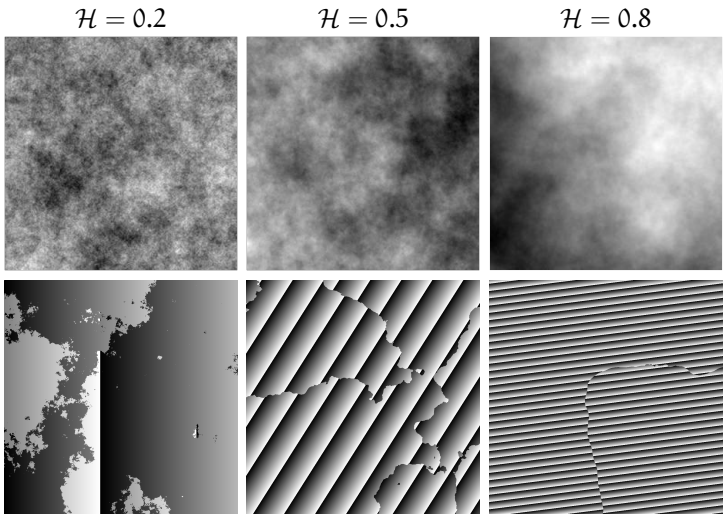

Fig. 3. Examples of MFBF samples. *Row 1: isotropic FBF* $\mathbf{F}_{\mathcal{H}}$ *associated with different Hurst parameters* $\mathcal{H}$*.. Row 2: phase terms of* $\mathbf{G}_{\mathcal{H},(u_0,v_0)}$.

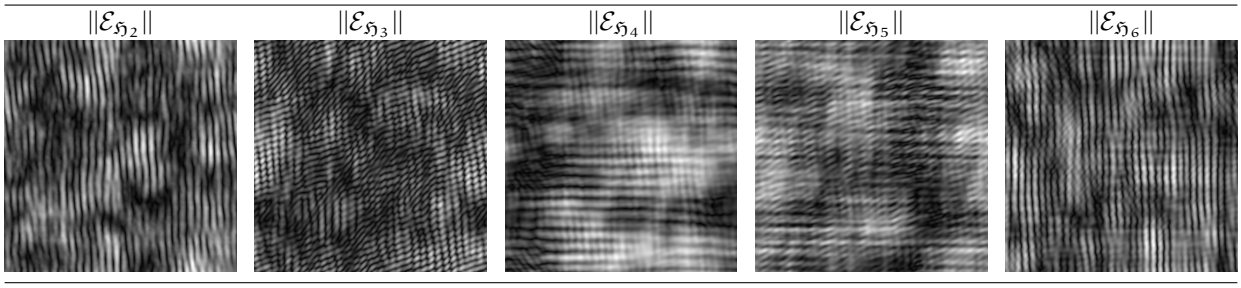

Fig. 4. GFBF samples $\mathcal{E}_{\mathfrak{H}_q}$ for $q = 2,3,4,5,6$. Texture $\mathcal{E}_{\mathfrak{H}_6}$ includes all features issued from $\mathcal{E}_{\mathfrak{H}_q}$, $q \leqslant 5$, whether these features are visible or not.

been defined in [1] as the stochastic Gaussian process with autocorrelation given by the convolution:

$$R_{\mathfrak{H}_Q} = \bigstar_{s=1}^{Q} R_{\mathbf{G}_{\mathcal{H}_s,(u_s,v_s)}} \tag{38}$$

GFBF $\mathcal{E}_{\mathfrak{H}_Q}$ can be seen as the spatial convolution, with respect to spatial variables, of Q independent MIFBF:

$$\mathcal{E}_{\mathfrak{H}_Q} = \bigstar_{s=1}^{Q} \mathbf{G}_{\mathcal{H}_s,(u_s,v_s)} \tag{39}$$

and this makes synthesis possible from convolution of samples of MIFBF (see examples of GFBF given by Figure 4). However, this convolution cannot be understood as a standard function operator since otherwise, non-regularity (due to stochasticity) and infinite energies (autocorrelation of MIFBF has fractional polynomial form) make straightforward calculus inefficient. The following section provides a mathematical sense to the convolution of two MIFBF in terms of integrals associated to kernel based measures.

B. On convolution of MIFBF (to GFBF)

The MIFBF is $\mathbf{G}_{\mathcal{H},(u_0,v_0)}(x,y) = e^{i(u_0x+v_0y)}\mathbf{F}_{\mathcal{H}}(x,y)$, a zero-mean Gaussian process with autocorrelation given by Eq. (37). We want to provide a sense to

$$\begin{aligned}&\mathbf{G}_{\mathcal{H}_1,(u_1,v_1)} \star \mathbf{G}_{\mathcal{H}_2,(u_2,v_2)}(t,s)\\ &= \int_{\mathbb{R}} \mathbf{G}_{\mathcal{H}_1,(u_1,v_1)}(x,y)\mathbf{G}_{\mathcal{H}_2,(u_2,v_2)}(t-x,s-y)d\mu(x,y)\end{aligned}$$

This sense will be associated to quadratic mean convergence. For the monovariate stochastic process case the complete steps of proof are given in Appendix B. Hereafter, we focus on the specific extension of Appendix B to the multivariate spatial case. The extension will be performed by:

- considering stochastic integrals

$$\mathbf{Y}_k(t,s) = \int_{\mathbb{R}} \mathbf{G}_{\mathcal{H}_k,(u_k,v_k)}(x,y)\, d\mu_{\Phi_{(t,s)}}(x,y) \quad (40)$$

- providing a quadratic mean sense to the following convolution of these integrals

$$\mathbf{Y}_1 \star \mathbf{Y}_2(t,s) = \int_{\mathbb{R}} \mathbf{Y}_1(x,y)\mathbf{Y}_2(t-x,s-y)dxdy$$

- associating the quadratic mean convergence of $\mathbf{G}_{\mathcal{H}_1,(u_1,v_1)} \star \mathbf{G}_{\mathcal{H}_2,(u_2,v_2)}$ to that of $\mathbf{Y}_1 \star \mathbf{Y}_2$ from properties of Φ.

The convergence of $\mathbf{Y}_1 \star \mathbf{Y}_2$ will be obtained hereafter by considering in Definition of Eq. (40), a *separable* measure $d\mu_{\Phi_{(\alpha,\beta)}}(x,y) = \phi_\alpha(x)\phi_\beta(y)dxdy$ where ϕ is the function described in Appendix B-A (having sufficiently fast decay in time and frequency). From this measure and by imposing that $\widehat{\phi}$ annihilates at frequencies $\pm(u_k,v_k)$: $\widehat{\phi}(\pm u_k) = \widehat{\phi}(\pm v_k) = 0$, we obtain:

1) Field $\mathbf{Y}(t,s)$ defined by Eq. (40) is a second order stochastic process : Indeed,

$$\begin{aligned}
&R_{\mathbf{Y}}(x,y,t,s) \\
&= \int_{\mathbb{R}^4} R_{\mathbf{G}_{\mathcal{H},(u,v)}}(x_1,x_2,y_1,y_2) \\
&\qquad d\mu_{\Phi_{(x,y)}}(x_1,y_1)d\mu_{\Phi_{(t,s)}}(x_2,y_2) \\
&= \int_{\mathbb{R}^4} R_{\mathbf{G}_{\mathcal{H},(u,v)}}(x_1,x_2,y_1,y_2)\phi_x(x_1)\phi_y(y_1) \\
&\qquad \phi_t(x_2)\phi_s(y_2)dx_1dx_2dy_1dy_2 \qquad (41)
\end{aligned}$$

where $R_{\mathbf{G}_{\mathcal{H},(u,v)}}$ is given by Eq. (37) and $(u,v) \in \{(u_1,v_1),(u_2,v_2)\}$. Let us analyze the 3 additive terms involved by expanding Eq. (37) in Eq. (41) separately. First

$$\begin{aligned}
&\int_{\mathbb{R}^4} e^{iu(x_1-y_1)}e^{iv(x_2-y_2)}\left(x_1^2+x_2^2\right)^{\mathcal{H}}\phi_x(x_1)\phi_y(y_1) \\
&\qquad \phi_t(x_2)\phi_s(y_2)dx_1dx_2dy_1dy_2 \\
&= \text{Constant} \times \widehat{\phi_y}(u)\widehat{\phi_s}(v) \\
&= \text{Constant} \times e^{-iyu}e^{-isv}\widehat{\phi}(u)\widehat{\phi}(v) \\
&= 0 \qquad (42)
\end{aligned}$$

Second

$$\begin{aligned}
&\int_{\mathbb{R}^4} e^{iu(x_1-y_1)}e^{iv(x_2-y_2)}\left(y_1^2+y_2^2\right)^{\mathcal{H}}\phi_x(x_1)\phi_y(y_1) \\
&\qquad \phi_t(x_2)\phi_s(y_2)dx_1dx_2dy_1dy_2 \\
&= \text{Constant} \times \widehat{\phi_x}(-u)\widehat{\phi_t}(-v) \\
&= \text{Constant} \times e^{-ixu}e^{-itv}\widehat{\phi}(-u)\widehat{\phi}(-v) \\
&= 0 \qquad (43)
\end{aligned}$$

Thus, $R_{\mathbf{Y}}$ reduces to the contribution of the third term, that is:

$$\begin{aligned}
&R_{\mathbf{Y}}(x,y,t,s) = \qquad (44) \\
&-\int_{\mathbb{R}^4} dx_1dx_2dy_1dy_2 e^{iu(x_1-y_1)}e^{iv(x_2-y_2)} \\
&\qquad \phi_x(x_1)\phi_y(y_1)\phi_t(x_2)\phi_s(y_2) \\
&\qquad \left[(x_1-y_1)^2+(x_2-y_2)^2\right]^{\mathcal{H}} \qquad (45)
\end{aligned}$$

and from a change of variable:

$$\begin{aligned}
&R_{\mathbf{Y}}(x,y,t,s) = \qquad (46) \\
&-\int_{\mathbb{R}^4} dz_1dz_2dy_1dy_2 e^{iuz_1}e^{ivz_2}\left[z_1^2+z_2^2\right]^{\mathcal{H}} \\
&\qquad \phi_x(z_1+y_1)\phi_y(y_1)\phi_t(z_2+y_2)\phi_s(y_2) \qquad (47)
\end{aligned}$$

which exists and is finite provided that $z^2\phi(z) \in L^1(\mathbb{R}) \cup L^2(\mathbb{R})$ (fast decay required for ϕ). In addition, after some steps of calculus similar to those of Appendix B-B, we derive:

$$\begin{aligned}
&R_{\mathbf{Y}}(x,y,t,s) \\
&= \frac{1}{4\pi^2}\int_{\mathbb{R}^2} e^{i(x-t)\omega_1}e^{i(y-s)\omega_2}\gamma_{\mathcal{H},(u,v)}(\omega_1,\omega_2) \qquad (48) \\
&\qquad \left|\widehat{\phi}(\omega_1)\right|^2\left|\widehat{\phi}(\omega_2)\right|^2 d\omega_1d\omega_2
\end{aligned}$$

where

$$\gamma_{\mathcal{H},(u,v)}(\omega_1,\omega_2) = \frac{\sigma^2 2^{1+2\mathcal{H}}\sin(\pi\mathcal{H})\Gamma^2(1+\mathcal{H})}{\left((\omega_1-u)^2+(\omega_2-v)^2\right)^{\mathcal{H}+1}} \qquad (49)$$

Thus, $R_{\mathbf{Y}}(x,y,t,s) = R_{\mathbf{Y}}(x-t,y-s)$ so that stationarity holds true for $\mathbf{Y}$ and we can use the following two-dimensional version for its autocorrelation:

$$\begin{aligned}
R_{\mathbf{Y}_k}(t,s) &= \frac{1}{4\pi^2}\int_{\mathbb{R}^2} e^{it\omega_1}e^{is\omega_2}\gamma_{\mathcal{H},(u,v)}(\omega_1,\omega_2) \\
&\qquad \left|\widehat{\phi}(\omega_1)\right|^2\left|\widehat{\phi}(\omega_2)\right|^2 d\omega_1d\omega_2 \qquad (50)
\end{aligned}$$

associated to the following PSD:

$$\begin{aligned}
&\gamma_{\mathbf{Y}}(\omega_1,\omega_2) \\
&= \gamma_{\mathcal{H},(u,v)}(\omega_1,\omega_2)\left|\widehat{\phi}(\omega_1)\right|^2\left|\widehat{\phi}(\omega_2)\right|^2 \qquad (51)
\end{aligned}$$

2) Convolution $\mathbf{Y}_1 \star \mathbf{Y}_2$ is a second order stochastic process: The convolution $\mathbf{Y}_1 \star \mathbf{Y}_2$ being with zero-mean, it is a well-defined second order process if $R_{\mathbf{Y}_1} \star R_{\mathbf{Y}_2}(x_1,x_2,y_1,y_2)$ exists and is finite for every

$x_1, x_2, y_1, y_2 \in \mathbb{R}$. Indeed, in this case:

$$\begin{aligned}
&\mathbb{E}\left[\mathbf{Y}_1 \star \mathbf{Y}_2(x_1,x_2)\,\overline{\mathbf{Y}_1 \star \mathbf{Y}_2(y_1,y_2)}\right] \\
&= \mathbb{E}\Bigg[\int_{\mathbb{R}^2} \mathbf{Y}_1(x,y)\mathbf{Y}_2(x_1-x,x_2-y)\mathrm{d}x\mathrm{d}y \\
&\qquad\qquad \overline{\int_{\mathbb{R}^2} \mathbf{Y}_1(t,s)\mathbf{Y}_2(y_1-t,y_2-s)\mathrm{d}t\mathrm{d}s}\Bigg] \\
&= \int_{\mathbb{R}^4} \mathrm{d}x\mathrm{d}y\mathrm{d}t\mathrm{d}s \mathbb{E}[\mathbf{Y}_1(x,y)\overline{\mathbf{Y}_1(t,s)}] \\
&\qquad\qquad \mathbb{E}[\mathbf{Y}_2(x_1-x,x_2-y)\overline{\mathbf{Y}_2(y_1-t,y_2-s)}] \\
&= \int_{\mathbb{R}^4} \mathrm{d}x\mathrm{d}y\mathrm{d}t\mathrm{d}s R_{\mathbf{Y}_1}(x,y,t,s) \\
&\qquad\qquad R_{\mathbf{Y}_2}(x_1-x,x_2-y,y_1-t,y_2-s) \\
&\triangleq R_{\mathbf{Y}_1} \star R_{\mathbf{Y}_2}(x_1,x_2,y_1,y_2) \qquad (52)
\end{aligned}$$

The existence of the convolution $R_{\mathbf{Y}_1} \star R_{\mathbf{Y}_2}$ of autocorrelation functions is thus the main criteria for providing a sense to the existence of $\mathbf{Y}_1 \star \mathbf{Y}_2$. Since $\mathbf{Y}_1$ and $\mathbf{Y}_2$ are stationary (see Section III-B1), we can focus on the two-dimensional versions of their autocorrelations. The problem then becomes the existence of:

$$R_{\mathbf{Y}_1} \star R_{\mathbf{Y}_2}(x,y) = \int_{\mathbb{R}^2} R_{\mathbf{Y}_1}(t,s)\, R_{\mathbf{Y}_2}(x-t,s-y)\mathrm{d}t\mathrm{d}s \quad (53)$$

where $R_{\mathbf{Y}_k}$ is given by Eq. (50). To solve this problem, we thus impose, in addition to annihilating frequencies $\pm(u_k,v_k)$, that $\widehat{\phi}$ is well localized in such a way that $\gamma_{\mathbf{Y}}$ defined by Eq. (51) belongs to $L^1(\mathbb{R}^2) \cap L^2(\mathbb{R}^2)$. In this respect, both $R_{\mathbf{Y}_1}$ and $R_{\mathbf{Y}_2}$ pertain to $L^1(\mathbb{R}^2) \cap L^2(\mathbb{R}^2)$ and we can conclude that $\mathbf{Y}_1 \star \mathbf{Y}_2$ is a second order stochastic field that converges in quadratic mean.

Moreover, we have from Eq. (53):

$$\begin{aligned}
&\gamma_{\mathbf{Y}_1 \star \mathbf{Y}_2}(\omega_1,\omega_2) \\
&= \gamma_{\mathbf{Y}_1}(\omega_1,\omega_2) \times \gamma_{\mathbf{Y}_2}(\omega_1,\omega_2) \\
&= \gamma_{\mathcal{H}_1,(u_1,v_1)}(\omega_1,\omega_2) \times \gamma_{\mathcal{H}_2,(u_2,v_2)}(\omega_1,\omega_2) \\
&\qquad \left|\times\widehat{\phi}(\omega_1)\right|^4 \times \left|\widehat{\phi}(\omega_2)\right|^4 \qquad (54)
\end{aligned}$$

The quadratic mean sense of $\mathbf{G}_{\mathcal{H}_1,(u_1,v_1)} \star \mathbf{G}_{\mathcal{H}_2,(u_2,v_2)}$ follows from the fact that we can provide a sequence $\left(\phi_t^{[n]}\right)_n$ (of wavelets for instance) where every $\phi_t^{[n]} \in L^1(\mathbb{R}) \cap L^2(\mathbb{R})$ which converges to a Dirac distribution: the result follows as a limit case and makes PSD association to $\mathbf{G}_{\mathcal{H}_1,(u_1,v_1)} \star \mathbf{G}_{\mathcal{H}_2,(u_2,v_2)}$ as (set $\widehat{\phi} = 1$ in Eq. (54)):

$$\begin{aligned}
&\gamma_{\mathbf{G}_{\mathcal{H}_1,(u_1,v_1)} \star \mathbf{G}_{\mathcal{H}_2,(u_2,v_2)}}(\omega_1,\omega_2) \\
&= \frac{\sigma_1^2 2^{1+2\mathcal{H}_1}\sin(\pi\mathcal{H}_1)\Gamma^2(1+\mathcal{H}_1)}{((\omega_1-u_1)^2+(\omega_2-v_1)^2)^{\mathcal{H}_1+1}} \\
&\qquad \times \frac{\sigma_2^2 2^{1+2\mathcal{H}_2}\sin(\pi\mathcal{H}_2)\Gamma^2(1+\mathcal{H}_2)}{((\omega_1-u_2)^2+(\omega_2-v_2)^2)^{\mathcal{H}_2+1}} \qquad (55)
\end{aligned}$$

Moreover, by iterating convolutions, we derive the PSD associated with a GFBF:

$$\begin{aligned}
&\gamma_{\mathcal{E}_{\mathcal{H}_Q}}(\omega_1,\omega_2) \\
&= \frac{\prod_{k=1}^{Q} \sigma_k^2 2^{1+2\mathcal{H}_k}\sin(\pi\mathcal{H}_k)\Gamma^2(1+\mathcal{H}_k)}{\prod_{k=1}^{Q}\left[(\omega_1-u_k)^2+(\omega_2-v_k)^2\right]^{\mathcal{H}_k+1}} \qquad (56)
\end{aligned}$$

PSD which highlights Q spectral poles when all couples (u_k,v_k) for $k = 1,2,\ldots Q$ are different.

IV. Multi-fractional PSD pole identification

Fractionally integrated fields presented in Sections II and III share one common property: they have PSD admitting many frequency points associated with infinite variances called poles. In practical applications requiring multi-fractional model selection, determining the number of interacting fields requires counting the number of frequency points with very high energy (exponential growth near the pole). Several solutions can be investigated for this problem. The easiest one involves selecting local maxima of the PSD and affecting them to poles. This has many drawbacks in terms of under- and over-determination (not any local maximum is effectively a pole and some poles can be squeezed when they are located near a pole with very high exponential growth).

We propose hereafter, after a long run search, a solution based on Convolutional Neural Network (CNN). The experimental setup concerns associating an observed multi-fractional GFBF[1] field to a category indexed by $Q \in \{1,2,\ldots\}$ corresponding to the number Q of poles used for sample generations.

The database generated for experimental tests contains 1200 images per specified value of Q: thus a total of 4800 GFBF images when the number of poles pertains to the category labels $\{1,2,3,4\}$. For any category, poles and Hurst parameters are generated randomly, following the gamma distribution so as to impose a significant energy concentration in $]0,\pi/2[\times]0,\pi/2[$ for poles and $]0,1/2[$ for Hurst exponents. An overview of this database[2], denoted $\mathcal{D}$ hereafter, is given by Figure 5.

A. Direct learning of multi-fractional texture features

Because multi-fractional interactions are obtained by convolution operators (filtering white noise so as to impose a desired structure), deep CNN architectures seems

[1] GFBF are chosen because their synthesis on the basis of fast Fourier transform requires less computational cost than the deluge of Γ computations for synthesis of K-DI-G fields.

[2] The complete database is available for download at: http://am.atto.free.fr/AlbumTexturesGFBF.htm.

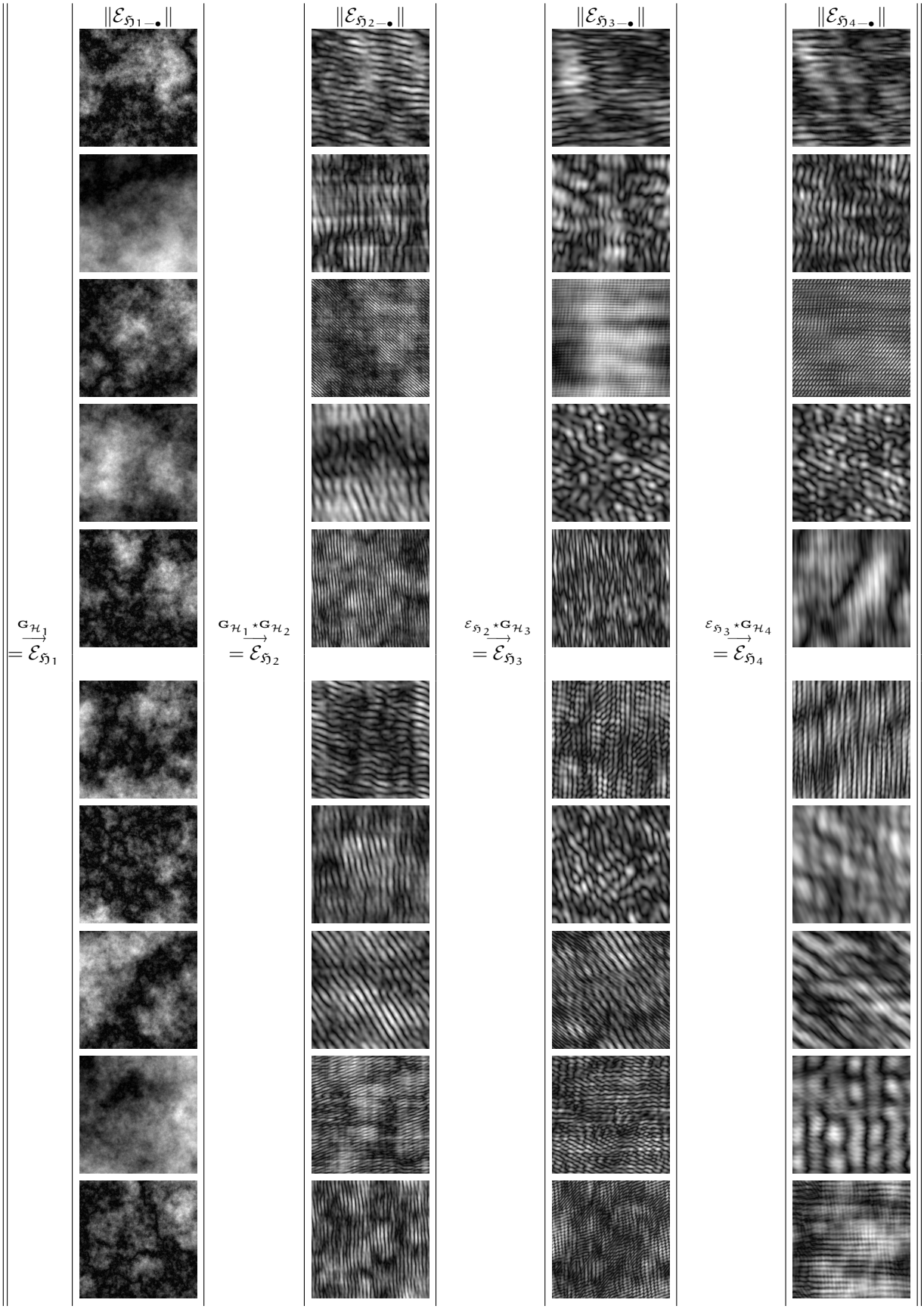

Fig. 5. Sample elements of GFBF database $\mathcal{D}$, where every $\mathcal{E}_{\mathfrak{H}_Q}$ is associated with a number Q of distinct poles.

adapted per nature[3] to their discrimination. In this respect, we have first investigated several existing architectures that are trained on millions of images to discriminate textures in $\mathcal{D}$ after retraining only the last convolutional layer. But none of them outruns more than 16% of good classification, the architecture achieving these 16% being "AlexNet" CNN [31] (trained on ImageNet [32], a database with 1000 categories and 1.2 million training images) which is known to yield more than 90% accuracy in standard image classification tasks!

These poor results are due to that multi-fractional textures are not objects with deterministic geometries: for the latter, feature recognition implies identifying similar structures up to elementary transformations whereas multi-fractional textures can present similar structures (Figure 5 shows almost more visual inter-category similarities than intra-category similarities), while having a different number of interactions: the issue is not thus a standard pattern recognition, but counting the number of visible pseudo-patterns.

We have thus been forced to retrain full CNNs by varying different features of the network. The most relevant architecture is still very close to [31], but with a significant improvement of convolution filter lengths to ensure the results given in Table I. These results are unsatisfactory and the conclusion has been seeking multi-fractional feature interactions from an indirect learning (see next section).

B. Indirect learning from PSD as inputs

As highlighted in the previous section, we have to force learning in not focusing on a recognized fractional feature since the same feature can appear in textures pertaining to different categories. For this purpose, we propose to perform learning of multi-fractional interactions from PSD features. Table II presents the best relevant results derived from the CNN described in Appendix C.

It follows from Table II that counting the number of multi-fractional interactions can be performed with good performance from CNN based approach associated with spectral inputs. A study of the first convolutional layer of the CNN shows specializations in 3 main convolution categories (see Figure 6):

- very selective filters in frequency and fast decay near the frequency selected (40% of first level convolution filters),
- selective filters in compact frequency blocks (rounded and wide support near the central frequency, 30% of first level convolution filters),
- multiple frequency selection filters (30% of first level convolution filters).

[3]Because they involve many layers of convolution filters and several non-linear transfer functions

Note that from Table II, increasing the number of interactions leads to a significant loss of performance. The reason is linked to the spectral content estimated from GFBF textures: 4 interactions means that 4 frequency points are associated with infinite variance (energy for zero-mean field) in $]0,\pi/2[\times]0,\pi/2[$. In addition, because of the exponential decays near these singular points, certain poles dominate others (the latter become almost non-visible in spectra as illustrated in Figure 7). Moreover, Figure 7 highlights that when the number of interactions is large, then:

- only few poles (bright values dominating their surrounding neighborhoods) are 'visible' in the PSD,
- the overlays of poles yield bright intersections that can be confused with poles.

V. Conclusion

The paper has shown that fractional order stochastic integration is a powerful tool for modeling with few parameters, image edge and texture information. Two categories of fractional field models corresponding to discrete and continuous domain integrals have been studied.

For discrete domain modeling, the main contribution proposed by the paper is the derivation of a category of fields where any field is associated with an arbitrary number of poles having their location controlled by a double indexed Gegenbauer polynomial.

For continuous domain modeling, the main contribution proposed by the paper is the proposal of a mathematical framework that provides a concise sense to convolutions of modulated fractional Brownian fields, any term involved in the convolution having the role of creating a spectral pole.

Because both discrete and continuous domain models can admit a pre-specified number of spectral poles, they are multi-fractional (a Holder exponent is associated with every pole) and this property raises the issue of counting the number of poles, given an image observation and for model selection purpose.

The paper has then proposed a third contribution consisting in providing a deep neural network architecture involving spectral information inputs and large size convolution filters at first network layers so as to make pole identification possible. This network is shown efficient for discriminating up to 4 neighbor poles, which is a good performance in a tricky problem: every pole is a spectral point associated with an infinite theoretical variance and its presence affects significantly the observability of other poles located in a close neighborhood.

Appendix A
Spatial Gegenbauer Fields

The problem expressed by Eq. (28) is expanding $\left(c-2\mu T-2\nu S+T^2+S^2\right)^{-\lambda}$ as a discrete series involv-

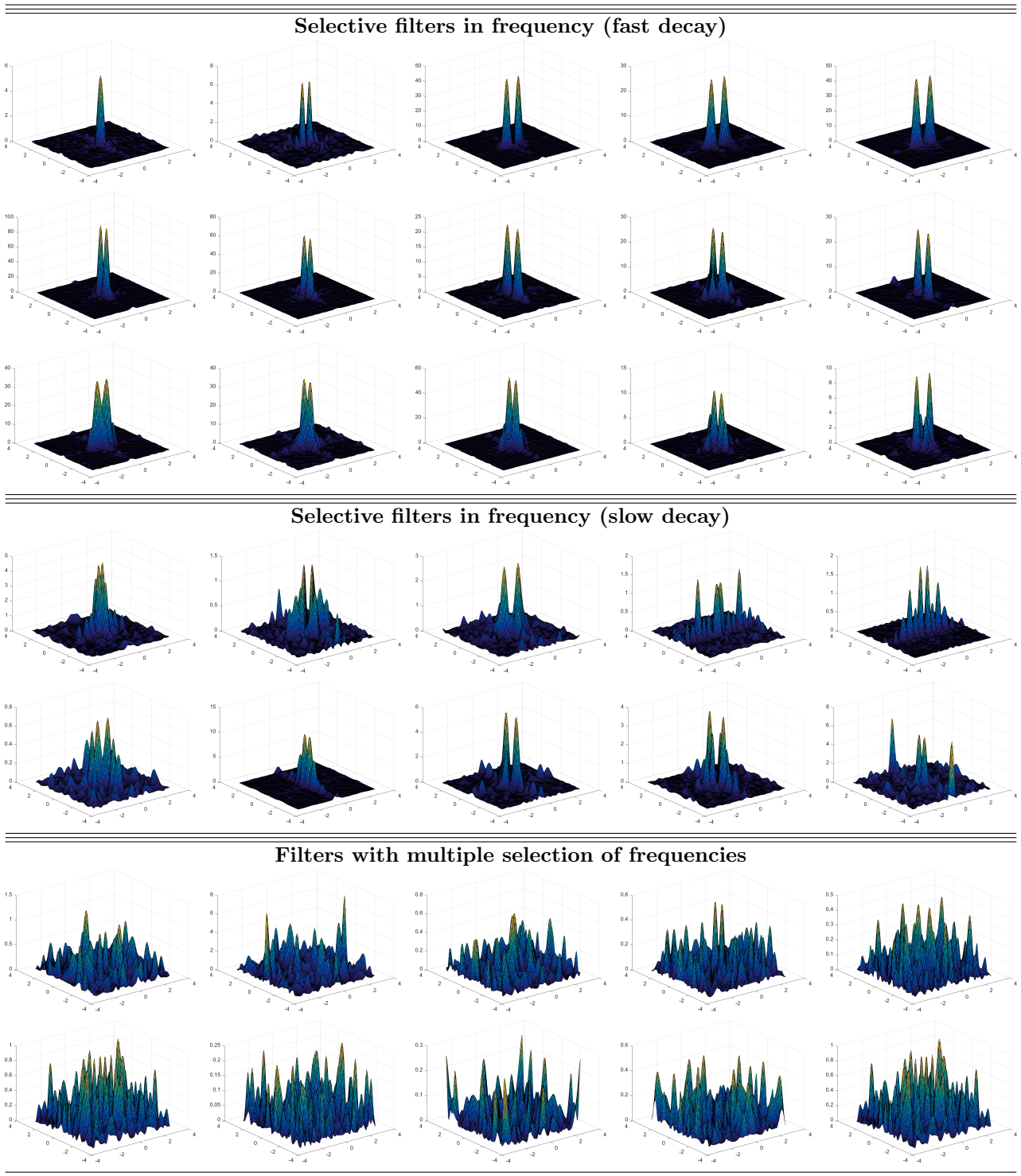

Fig. 6. First convolutional layer of the CNN network described in C when learning has been addressed from GFBF PSD features.

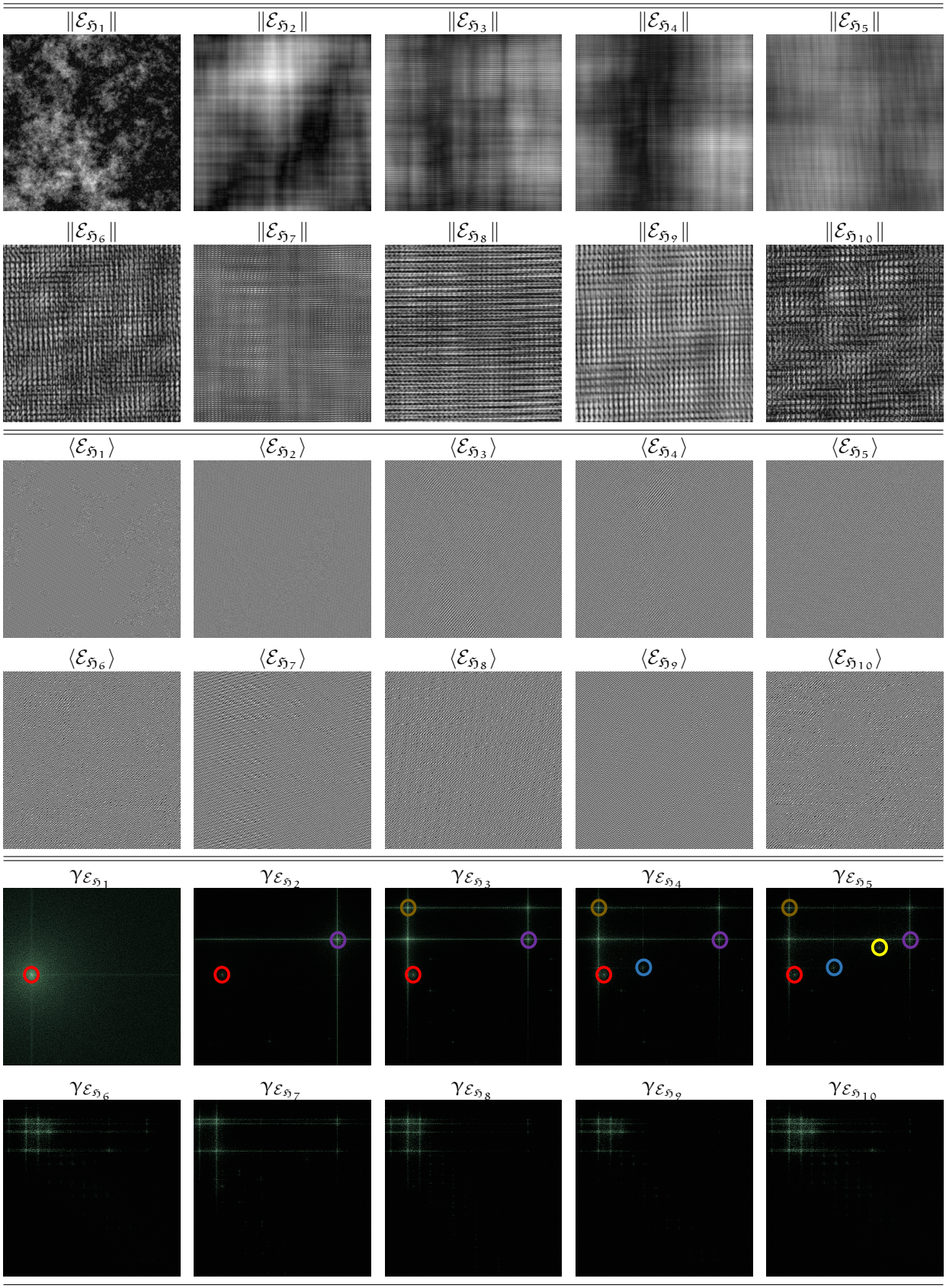

Fig. 7. Curse of power for GFBF $\mathcal{E}_{\mathfrak{H}_Q}$ associated with PSD $\gamma_{\mathcal{E}_{\mathfrak{H}_Q}}$: PSD is displayed as $\log(1+\log(1+\text{WP Spectrum}))$ to allow observing some poles. But when the number of interactions is high, only the few dominant poles are visible in the PSD! [Sizes] / Input GFBF: 4092×4092 ; GFBF PSD: 1024×1024 ; Supports displayed: $64 \times 64 \longmapsto [0, \pi/16] \times [0, \pi/16]$.

ing integer powers of T and S. This can be done by noting that the *Gamma* function given by Eq. (13) has equivalent expression (change of variable $u \rightarrow \left(c - 2\mu T - 2\nu S + T^2 + S^2\right) x$):

$$\Gamma(\lambda) = \left(c - 2\mu T - 2\nu S + T^2 + S^2\right)^{\lambda} \times \int_0^{+\infty} e^{-\left(c-2\mu T-2\nu S+T^2+S^2\right)x} x^{\lambda-1} dx \quad (57)$$

so that we can write:

$$\left(c - 2\mu T - 2\nu S + T^2 + S^2\right)^{-\lambda} = \frac{1}{\Gamma(\lambda)} \int_0^{+\infty} e^{-cx} x^{\lambda-1} e^{\left(2\mu T - T^2\right)x} e^{\left(2\nu S - S^2\right)x} dx$$

The latter can be written in terms of the Hermite-Kampé de Fériet polynomials [33]:

$$\left(c - 2\mu T - 2\nu S + T^2 + S^2\right)^{-\lambda} = \frac{1}{\Gamma(\lambda)} \sum_{m=0}^{\infty} \sum_{n=0}^{\infty} \frac{1}{m!\ n!} T^m S^n \times \left(\int_0^{+\infty} e^{-cx} x^{\lambda-1} H_m(2\mu x, -x) H_n(2\nu x, -x) dx \right)$$

where

$$H_k(x, y) = k! \sum_{j=0}^{\lfloor k/2 \rfloor} \frac{x^{k-2j} y^j}{(k-2j)!\ j!} \quad (58)$$

Thus

$$\left(c - 2\mu T - 2\nu S + T^2 + S^2\right)^{-\lambda} = \sum_{m=0}^{\infty} \sum_{n=0}^{\infty} C_{m,n}^{\lambda}(\mu, \nu) T^m S^n \quad (59)$$

with

$$C_{m,n}^{\lambda}(\mu, \nu) = \frac{1}{m!\ n!} \frac{1}{c^{\lambda+m+n}} \qquad \frac{1}{\Gamma(\lambda)} \times \left(\int_0^{+\infty} e^{-x} x^{\lambda-1} H_m(2\mu x, -cx) H_n(2\nu x, -cx) dx \right) \quad (60)$$

Now, by using Eq. (58), we derive that:

$$\int_0^{+\infty} e^{-x} x^{\lambda-1} H_m(2\mu x, -cx) H_n(2\nu x, -cx) dx = m!\ n! \sum_{p=0}^{\lfloor m/2 \rfloor} \sum_{q=0}^{\lfloor n/2 \rfloor} \frac{(2\mu)^{m-2p} (2\nu)^{n-2q} (-c)^{p+q}}{(m-2p)!\ (n-2q)!\ p!\ q!} \times \int_0^{+\infty} e^{-x} x^{\lambda+m-p+n-q-1} dx$$

which, by noting that

$$\int_0^{+\infty} e^{-x} x^{\lambda+m-p+n-q-1} dx = \Gamma(\lambda + m + n - p - q)$$

leads us to conclude that Eq. (60) is equivalent to:

$$C_{m,n}^{\lambda}(\mu, \nu) = \frac{1}{c^{\lambda+m+n}} \frac{1}{\Gamma(\lambda)} \times \sum_{p=0}^{\lfloor m/2 \rfloor} \sum_{q=0}^{\lfloor n/2 \rfloor} \Gamma(\lambda + m + n - p - q) \times \frac{(-1)^{p+q} c^{p+q} (2\mu)^{m-2p} (2\nu)^{n-2q}}{p!\ q!\ (m-2p)!\ (n-2q)!} \quad (61)$$

In particular, when b=1, we note $C_{m,n}^{1} \triangleq C_{m,n}$, which reduces to:

$$C_{m,n}(\mu, \nu) = \frac{1}{c^{1+m+n}} \times \sum_{p=0}^{\lfloor m/2 \rfloor} \sum_{q=0}^{\lfloor n/2 \rfloor} (m + n - p - q)! \times \frac{(-1)^{p+q} c^{p+q} (2\mu)^{m-2p} (2\nu)^{n-2q}}{p!\ q!\ (m-2p)!\ (n-2q)!} \quad (62)$$

since $\Gamma(1) = 1$ and $\Gamma(k+1) = k!$ when k is a non-negative integer.

Appendix B
On convolutions of modulated fractional Brownian motions

A. Context

Consider a stochastic zero-mean process: $\mathbf{X} : (t, \lambda) \in \mathbb{R} \times \Omega$ or $\mathbb{Z} \times \Omega \longmapsto \mathbf{X}(t, \omega) = \mathbf{X}(t, \lambda) = \mathbf{X}_t(\lambda) = \mathbf{X}_\lambda(t) \triangleq \mathbf{X}(t) \in \mathbb{R}$. Assuming that $\mathbf{X}$ is a second-order stochastic means, for all t:

$$\|\mathbf{X}(t)\|_{L^2(\Omega)}^2 = \mathbb{E}\left[|\mathbf{X}(t)|^2\right] = \int_{\Omega} |\mathbf{X}(t)|^2 dP(\lambda) < \infty \quad (63)$$

where $\Omega = \mathbb{R}$ in the following and P is a probability measure on elements of $\mathcal{B}(\mathbb{R})$. Under property given by Eq. (63), functions [mean]: $t \mapsto \mathbb{E}\mathbf{X}(t)$ and [autocorrelation] $(t, s) \mapsto \mathbb{E}[\mathbf{X}(t)\,\mathbf{X}(s)] = R(t, s)$ are well-defined and real valued.

For a second-order stochastic process, continuity (that is $\mathbf{X}(t) \rightarrow \mathbf{X}(s)$ as $t \rightarrow s$) is related to the so-called *quadratic mean* sense (use of the norm associated to $L^2(\Omega)$) and consists in:

$$\lim_{t \to s} \|\mathbf{X}(t) - \mathbf{X}(s)\|_{L^2(\Omega)}^2 = \lim_{t \to s} \mathbb{E}|\mathbf{X}(t) - \mathbf{X}(s)|^2 = 0$$

A consequence of using the quadratic norm is the following: $\mathbf{X}$ is continuous (in quadratic mean) if functions $t \mapsto \mathbb{E}\mathbf{X}(t)$ and $(t, s) \mapsto \mathbb{E}[\mathbf{X}(t)\,\mathbf{X}(s)] = R(t, s)$ are continuous (standard function continuity). We assume that $\mathbf{X}$ is with zero-mean in what follows.

A second-order zero-mean stochastic Gaussian process is completely specified by its autocorrelation function. For the Fractional Brownian Motion (FBM) denoted $\mathbf{X}_{\mathcal{H}}$ with Hurst exponent/parameter $\mathcal{H}$, $0 < \mathcal{H} < 1$, this autocorrelation function is given by:

$$R_{\mathcal{H}}(t, s) = \frac{\sigma^2}{2} \left(|t|^{2\mathcal{H}} + |s|^{2\mathcal{H}} - |t - s|^{2\mathcal{H}} \right) \quad (64)$$

The FBM Modulation (FBMM) by a deterministic exponential wave, denoted $\mathbf{X}_{\mathcal{H},u_0}(x) = e^{iu_0 x}\mathbf{X}_{\mathcal{H}}(x)$ is a Gaussian process with zero-mean (as a consequence of zero-mean assumption on $\mathbf{X}_{\mathcal{H}}$) and autocorrelation:

$$\begin{aligned} R_{\mathbf{X}_{\mathcal{H},u_0}}(t,s) &= \mathbb{E}[\mathbf{X}_{\mathcal{H},u_0}(t)\,\overline{\mathbf{X}_{\mathcal{H},u_0}(s)}] \\ &= e^{iu_0(t-s)}R_{\mathcal{H}}(t,s) \end{aligned} \tag{65}$$

where $R_{\mathcal{H}}$ is given by Eq. (64).

Consider now two independent FBMM $\mathbf{X}_{\mathcal{H}_1,u_1}$ and $\mathbf{X}_{\mathcal{H}_2,u_2}$. We want to provide a quadratic mean sense to the following convolution operator between FBMM:

$$\begin{aligned} &\mathbf{X}_{\mathcal{H}_1,u_1} \star \mathbf{X}_{\mathcal{H}_2,u_2}(t) \\ &\quad \stackrel{?}{=} \int_{\mathbb{R}} \mathbf{X}_{\mathcal{H}_1,u_1}(x)\mathbf{X}_{\mathcal{H}_2,u_2}(t-x)d\mu(x) \end{aligned} \tag{66}$$

In practice, if we assume that μ is the Lebesgue's measure, it would have been sufficed that $R_{\mathbf{X}_{\mathcal{H}_1,u_1}}$ and $R_{\mathbf{X}_{\mathcal{H}_2,u_2}}$ pertain to $L^2(\mathbb{R}^2)$. However, this is not true for FBMM as it can be observed by taking Eq. (64) and Eq. (65) into account. Nevertheless, we can go beyond these functional limitations by selecting an appropriate parametric measure that transforms $\mathbf{X}_{\mathcal{H}_1,u_1}$ and $\mathbf{X}_{\mathcal{H}_2,u_2}$ into $\mathbf{Y}_1$ and $\mathbf{Y}_2$:

$$\mathbf{Y}_k(t) \triangleq \int_{\mathbb{R}} \mathbf{X}_{\mathcal{H}_k,u_k}(x)\,d\mu_t(x) \tag{67}$$

for $k = 1,2$ and with convergence of the latter integrals in quadratic mean sense. Note that for the convergence of Eq. (67) to hold true, it suffices to provide a kernel ϕ satisfying

- $\phi \in L^1(\mathbb{R}) \cup L^2(\mathbb{R})$,
- $(1+x^2)\phi(x) \in L^1(\mathbb{R}) \cup L^2(\mathbb{R})$,

and let $d\mu_t(x) = \phi_t(x)dx$ where $\phi_t(x) = \phi(x-\lambda t)$. For such a measure,

$$\int_{\mathbb{R}^2} e^{iu_0(x-y)}|x|^{2\mathcal{H}_k}\phi_t(x)\phi_s(y)dxdy$$

and

$$\int_{\mathbb{R}^2} e^{iu_0(x-y)}|x-y|^{2\mathcal{H}_k}\phi_t(x)\phi_s(y)dxdy$$

exists and are finite, thus,

$$\begin{aligned} \|\mathbf{Y}_k(t)\|^2_{L^2(\Omega)} &\triangleq \left\| \int_{\mathbb{R}} \mathbf{X}_{\mathcal{H}_k,u_k}(x)\,d\mu_t(x) \right\|^2_{L^2(\Omega)} \\ &= \int_{\mathbb{R}^2} R_{\mathbf{X}_{\mathcal{H}_k,u_k}}(x,y)\phi_t(x)\phi_s(y)dxdy \\ &< \infty \end{aligned}$$

in case where $R_{\mathbf{X}_{\mathcal{H}_k,u_k}}$ has the form given by Eq. (65). The quadratic mean sense of $\mathbf{X}_{\mathcal{H}_k,u_k}$ follows from this last property as a limit case, given that we can provide sequence $\left(\phi_t^{[n]}\right)_n$ such as wavelets where every $\phi_t^{[n]} \in L^1(\mathbb{R}) \cap L^2(\mathbb{R})$ and parameterized by an upper index n which makes them converge to Dirac distributions.

B. PSD association to FBMM $\mathbf{X}_{\mathcal{H}_k,u_k}$ via that of $\mathbf{Y}_k$

In the following, we assume that the following property holds true for k=1, 2:

> [**Blocking frequency** $\pm u_k$] function ϕ introduced in section above satisfies at the specific real values $\pm u_k$: $\widehat{\phi}(u_k) = \widehat{\phi}(-u_k) = 0$

where we have used the following definition of the Fourier transform:

$$\widehat{\phi}(\omega) = \int_{\mathbb{R}} e^{-i\omega x}\phi(x)dx \tag{68}$$

Consider the autocorrelation function $R_{\mathbf{Y}_k}$ of $\mathbf{Y}_k$:

$$\begin{aligned} R_{\mathbf{Y}_k}(t,s) &= \int_{\mathbb{R}^2} R_{\mathbf{X}_{\mathcal{H}_k,u_k}}(x,y)\phi_t(x)\phi_s(y)dxdy \\ &= \frac{\sigma^2}{2}\int_{\mathbb{R}^2} \left(|x|^{2\mathcal{H}_k} + |y|^{2\mathcal{H}_k} - |x-y|^{2\mathcal{H}_k}\right) \\ &\qquad e^{iu_k(x-y)}\phi_t(x)\phi_s(y)dxdy \end{aligned} \tag{69}$$

Under frequency $\pm u_k$ blocking by ϕ, we obtain:

$$R_{\mathbf{Y}_k}(t,s) = -\frac{\sigma^2}{2}\int_{\mathbb{R}^2} e^{iu_k(x-y)}|x-y|^{2\mathcal{H}_k}\phi_t(x)\phi_s(y)dxdy$$

This integral can be re-written, from a change of variable:

$$R_{\mathbf{Y}_k}(t,s) = -\frac{\sigma^2}{2}\int_{\mathbb{R}^2} e^{iu_k z}|z|^{2\mathcal{H}_k}\phi_t(z+y)\phi_s(y)dzdy$$

By decomposing $|z|^{2\mathcal{H}_k}$ with respect to [34], we deduce:

$$\begin{aligned} R_{\mathbf{Y}_k}(t,s) &= -\frac{\sigma^2}{2}\frac{\Gamma(2\mathcal{H}+1)\sin(\pi\mathcal{H})}{\pi}\times \\ &\int_{\mathbb{R}^2} e^{iu_k z}\left(\int_{\mathbb{R}} \frac{1-\cos(z\xi)}{|\xi|^{2\mathcal{H}_k+1}}d\xi\right)\phi_t(z+y)\phi_s(y)dzdy \end{aligned} \tag{70}$$

and by noting:

$$\gamma_{\mathcal{H}}(\xi) = \frac{\sigma^2\Gamma(2\mathcal{H}+1)\sin(\pi\mathcal{H})}{|\xi|^{2\mathcal{H}+1}} \tag{71}$$

we derive:

$$\begin{aligned} &R_{\mathbf{Y}_k}(t,s) = \\ &-\frac{1}{2\pi}\int_{\mathbb{R}} \gamma(\xi)d\xi\times \\ &\qquad \int_{\mathbb{R}^2} e^{iu_k z}\left(1-\cos(z\xi)\right)\phi_t(z+y)\phi_s(y)dzdy \end{aligned} \tag{72}$$

By taking again into account, the kernel ϕ frequency $\pm u_k$ blocking property, we have:

$$\int_{\mathbb{R}^2} e^{iu_k z}\phi_t(z+y)\phi_s(y)dzdy = e^{iu_k(t-s)}\widehat{\phi}(-u_k)\widehat{\phi}(u_k) = 0$$

and thus:

$$\begin{aligned} R_{\mathbf{Y}_k}(t,s) &= \frac{1}{2\pi}\times \\ &\int_{\mathbb{R}} d\xi\gamma(\xi)\int_{\mathbb{R}^2} e^{iu_k z}\cos(z\xi)\phi_t(z+y)\phi_s(y)dzdy \end{aligned} \tag{73}$$

which is equivalent to

$$\begin{aligned} R_{\mathbf{Y}_k}(t,s) &= \frac{1}{2\pi}\times \\ &\int_{\mathbb{R}} d\xi\gamma(\xi)\int_{\mathbb{R}^2} e^{iu_k z}\frac{e^{iz\xi}+e^{-iz\xi}}{2}\phi_t(z+y)\phi_s(y)dzdy \end{aligned}$$

The latter corresponds, after some Fourier based calculus:

$$R_{\mathbf{Y}_k}(t,s) = \frac{1}{2\pi}\int_{\mathbb{R}} d\xi\gamma(\xi)\frac{1}{2}\times \left(\widehat{\phi_t}(-\xi-u_k)\overline{\widehat{\phi_s}}(-\xi-u_k) + \widehat{\phi_t}(\xi-u_k)\overline{\widehat{\phi_s}}(\xi-u_k)\right)$$

thus,

$$R_{\mathbf{Y}_k}(t,s) = \frac{1}{2\pi}\int_{\mathbb{R}} \gamma(\xi+u_k)\widehat{\phi_t}(\xi)\overline{\widehat{\phi_s}}(\xi)d\xi$$

Now, since we have assumed that t in notation ϕ_t denotes a translation parameter, then: $\widehat{\phi_t}(\xi) = e^{-ict\xi}\widehat{\phi}(\xi)$ and $\widehat{\phi_s}(\xi) = e^{-ics\xi}\widehat{\phi}(\xi)$ so that:

$$R_{\mathbf{Y}_k}(t,s) = \frac{1}{2\pi}\int_{\mathbb{R}} \gamma(\xi+u_k)e^{-ic(t-s)\xi}\left|\widehat{\phi}(\xi)\right|^2 d\xi$$

and finally:

$$R_{\mathbf{Y}_k}(t,s) = \frac{1}{2\pi}\int_{\mathbb{R}} \gamma(\xi-u_k)e^{ic(t-s)\xi}\left|\widehat{\phi}(\xi)\right|^2$$

which converges provided that $\sup_{|\xi-u_k|\leqslant\eta}\left|\widehat{\phi}(\xi)/\xi\right| < \infty$ for some $\eta > 0$. In this case, $\mathbf{Y}_k$ is a stationary[4] stochastic process with autocorrelation in the reduced one-dimensional form:

$$R_{\mathbf{Y}_k}(t) = \frac{1}{2\pi}\int_{\mathbb{R}} \gamma(\xi-u_k)\left|\widehat{\phi}(\xi)\right|^2 e^{ict\xi}d\xi$$

and associated with PSD (derived from inverse Fourier identification in the latter form):

$$\gamma_{\mathbf{Y}_k}(\xi) = \gamma(\xi-u_k)\left|\widehat{\phi}(\xi)\right|^2$$

Assuming that ideal ϕ behaves approximately as a Dirac distribution (limit case as discussed at the end of the previous section), we can associate the following PSD to $\mathbf{X}_k$:

$$\gamma_{\mathbf{X}_k}(\xi) = \gamma(\xi-u_k) = \frac{\sigma^2\Gamma(2\mathcal{H}+1)\sin(\pi\mathcal{H})}{|\xi-u_k|^{2\mathcal{H}+1}}$$

C. Convolution between FBMM $\mathbf{X}_{\mathcal{H}_1,u_1}, \mathbf{X}_{\mathcal{H}_2,u_2}$ via characterization of $\mathbf{Y}_1 \star \mathbf{Y}_2$

The sole condition required for the convolution

$$\int_{\mathbb{R}} \mathbf{Y}_1(x)\mathbf{Y}_2(t-x)dx \triangleq \mathbf{Y}_1 \star \mathbf{Y}_2(t)$$

to make sense as the definition of a second order stochastic process $\mathbf{Y}_1 \star \mathbf{Y}_2$ is the existence of:

$$\begin{aligned}&\iint \mathbb{E}[\mathbf{Y}_1(x)\mathbf{Y}_2(t-x)\overline{\mathbf{Y}_1(y)\mathbf{Y}_2(s-y)}]dxdy\\ &= \iint \mathbb{E}[\mathbf{Y}_1(x)\overline{\mathbf{Y}_1(y)}]\mathbb{E}[\mathbf{Y}_2(t-x)\overline{\mathbf{Y}_2(s-y)}]dxdy\\ &= \iint R_{\mathbf{Y}_1}(x,y)R_{\mathbf{Y}_2}(t-x,s-y)dxdy\\ &= R_{\mathbf{Y}_1}\star R_{\mathbf{Y}_2}(t,s)\end{aligned} \tag{74}$$

If $R_{\mathbf{Y}_1}, R_{\mathbf{Y}_2} \in L^2(\mathbb{R}^2)$, then this condition is satisfied. The latter is not very restrictive since ϕ can be chosen well-localized in time frequency.

Furthermore, under the stationarity induced by ϕ-measure on $\mathbf{Y}_1, \mathbf{Y}_2$, then:

- from the change of variable $t \leftarrow t-s$ and $x \leftarrow x-y$, we can write:
$$R_{\mathbf{Y}_1\star\mathbf{Y}_2}(t) = \int R_{\mathbf{Y}_1}(x)R_{\mathbf{Y}_2}(t-x)dx$$
- and, provided that $R_{\mathbf{Y}_1\star\mathbf{Y}_2}$ obtained just above admits a Fourier transform, we can deduce the PSD $\gamma_{\mathbf{Y}_1\star\mathbf{Y}_2}$ of $\mathbf{Y}_1 \star \mathbf{Y}_2$ as:
$$\begin{aligned}\gamma_{\mathbf{Y}_1\star\mathbf{Y}_2}(\xi) &= \int R_{\mathbf{Y}_1}\star R_{\mathbf{Y}_2}(t)e^{-i\xi t}dt\\ &= \gamma_{\mathbf{Y}_1}(\xi)\gamma_{\mathbf{Y}_2}(\xi)\\ &= \gamma(\xi-u_1)\gamma(\xi-u_2)\left|\widehat{\phi}(\xi)\right|^4\end{aligned} \tag{75}$$

Finally, the PSD associated[5] to $\mathbf{X}_{\mathcal{H}_1,u_1} \star \mathbf{X}_{\mathcal{H}_2,u_2}$ *via* kernel ϕ is:

$$\begin{aligned}&\gamma_{\mathbf{X}_{\mathcal{H}_1,u_1}\star\mathbf{X}_{\mathcal{H}_2,u_2}}(\xi)\\ &= \gamma(\xi-u_1)\gamma(\xi-u_2)\\ &= \gamma_{\mathbf{X}_{\mathcal{H}_1,u_1}}(\xi)\times\gamma_{\mathbf{X}_{\mathcal{H}_2,u_2}}(\xi)\\ &= \frac{\sigma_1^2\sigma_2^2\Gamma(2\mathcal{H}_1+1)\Gamma(2\mathcal{H}_2+1)\sin(\pi\mathcal{H}_1)\sin(\pi\mathcal{H}_2)}{|\xi-u_1|^{2\mathcal{H}_1+1}|\xi-u_2|^{2\mathcal{H}_2+1}}\end{aligned}$$

Appendix C
Convolutional Neural Network (CNN) architecture for multi-fractional pole identification

The CNN proposed for multi-fractional interaction count is presented in Table III. This CNN is characterized by a first convolution layer with long-size impulse response filters so as to possibly allows for a concise frequency selection and surprisingly, up to 40% of the filters have been specialized (starting from a white noise initialization) in frequency selection (see Figure 6).

In the CNN of Table III, sizes of convolution filters have been decreased progressively, from layer to layer, in order

[4]For a zero-mean second order stochastic process $\mathbf{X}$, stationarity (second-order or Wide Sense Stationarity, WSS) holds true if:

$$R_{\mathbf{X}}(t,s) = R_{\mathbf{X}}(t-s,0) \equiv R_{\mathbf{X}}(t-s=x)$$

[5]Deduction must be understood as a limit case involving an $L^1(\mathbb{R})\cap L^2(\mathbb{R})$ sequence $\left(\phi_t^{[n]}\right)_n$ that converges to a Dirac distribution, thus $\left(\widehat{\phi_t^{[n]}}\right)_n$ tends to constant function 1.

to limit the overall CNN complexity. From Table III, we have the following correspondences:

- Rectified Linear Unit (ReLU), function

$$x \mapsto (x)_+ = \begin{cases} x & \text{if} \quad x > 0 \\ 0 & \text{if} \quad x \leqslant 0 \end{cases}$$

- Normalization (cross-channel):

$$x_m \mapsto y_m = x_m \left(\kappa + \alpha \sum_{\max\{0, m-n/2\}}^{\max\{N-1, m+n/2\}} x_\ell^2 \right)^{-\beta}$$

  where N is the number of kernels used in the layer and n is the normalization neighborhood size (same spatial position, n adjacent channels);
- Softmax:

$$X = (X_i)_{i=1}^n \mapsto \left(e^{X_i} / \sum_{i=1}^n e^{X_i} \right)_{i=1}^n$$

  this loss function is used for the prediction of a single category between Q mutually exclusive Q-fractional categories.

References

[1] A. M. Atto, Z. Tan, O. Alata, and M. Moreaud, "Non-stationary texture synthesis from random field modeling," in *IEEE International Conference on Image Processing (ICIP)*, Oct 2014, pp. 4266–4270.

[2] K. Polisano, M. Clausel, V. Perrier, and L. Condat, "Texture modeling by gaussian fields with prescribed local orientation," in *2014 IEEE International Conference on Image Processing (ICIP)*, Oct 2014, pp. 6091–6095.

[3] D. P. Kroese and Z. I. Botev, "Spatial process generation," *arXiv* eprint available at http://arxiv.org/abs/1308.0399, 2013.

[4] Y. F. Pu, J. L. Zhou, and X. Yuan, "Fractional differential mask: A fractional differential-based approach for multiscale texture enhancement," *IEEE Transactions on Image Processing*, vol. 19, no. 2, pp. 491–511, Feb 2010.

[5] T. Lundahl, W. J. Ohley, S. M. Kay, and R. Siffert, "Fractional brownian motion: A maximum likelihood estimator and its application to image texture," *IEEE Transactions on Medical Imaging*, vol. 5, no. 3, pp. 152–161, Sept 1986.

[6] P. Kube and A. Pentland, "On the imaging of fractal surfaces," *IEEE Transactions on Pattern Analysis and Machine Intelligence*, vol. 10, no. 5, pp. 704–707, Sep 1988.

[7] C. V. Stewart, B. Moghaddam, K. J. Hintz, and L. M. Novak, "Fractional brownian motion models for synthetic aperture radar imagery scene segmentation," *Proceedings of the IEEE*, vol. 81, no. 10, pp. 1511–1522, Oct 1993.

[8] L. M. Kaplan and C. C. J. Kuo, "An improved method for 2-d self-similar image synthesis," *IEEE Transactions on Image Processing*, vol. 5, no. 5, pp. 754 – 761, May 1996.

[9] B. Pesquet-Popescu, "Wavelet packet decompositions for the analysis of 2-d fields with stationary fractional increments," *IEEE Transactions on Information Theory*, vol. 45, no. 3, pp. 1033 – 1039, Apr. 1999.

[10] L. M. Kaplan, "Extended fractal analysis for texture classification and segmentation," *IEEE Transactions on Image Processing*, vol. 8, no. 11, pp. 1572 – 1585, Nov. 1999.

[11] A. I. Penn and M. H. Loew, "Estimating fractal dimension with fractal interpolation function models," *IEEE Transactions on Medical Imaging*, vol. 16, no. 6, pp. 930–937, Dec 1997.

[12] A. S. Balghonaim and J. M. Keller, "A maximum likelihood estimate for two-variable fractal surface," *IEEE Transactions on Image Processing*, vol. 7, no. 12, pp. 1746–1753, Dec 1998.

[13] B. Pesquet-Popescu and J.-C. Pesquet, "Synthesis of bidimensional α-stable models with long-range dependence," *Signal Processing, Elsevier*, vol. 82, no. 12, pp. 1927 – 1940, 2002.

[14] K. B. Eom, "Long-correlation image models for textures with circular and elliptical correlation structures," *IEEE Transactions on Image Processing*, vol. 10, no. 7, pp. 1047–1055, July 2001.

[15] R. Jennane, W. J. Ohley, S. Majumdar, and G. Lemineur, "Fractal analysis of bone x-ray tomographic microscopy projections," *IEEE Transactions on Medical Imaging*, vol. 20, no. 5, pp. 443–449, May 2001.

[16] P. Campisi, E. Maiorana, A. Neri, and G. Scarano, "Video texture modelling and synthesis using fractal processes," *IET Image Processing*, vol. 2, no. 1, pp. 1–17, Feb 2008.

[17] K. P. Hollingsworth, K. W. Bowyer, and P. J. Flynn, "The best bits in an iris code," *IEEE Transactions on Pattern Analysis and Machine Intelligence*, vol. 31, no. 6, pp. 964–973, June 2009.

[18] A. M. Atto, Y. Berthoumieu, and P. Bolon, "2-d wavelet packet spectrum for texture analysis," *Image Processing, IEEE Transactions on*, vol. 22, no. 6, pp. 2495–2500, 2013.

[19] Y. F. Pu, "Fractional-order euler-lagrange equation for fractional-order variational method: A necessary condition for fractional-order fixed boundary optimization problems in signal processing and image processing," *IEEE Access*, vol. 4, pp. 10 110–10 135, 2016.

[20] S. Combrexelle, H. Wendt, N. Dobigeon, J. Y. Tourneret, S. McLaughlin, and P. Abry, "Bayesian estimation of the multifractality parameter for image texture using a whittle approximation," *IEEE Transactions on Image Processing*, vol. 24, no. 8, pp. 2540–2551, Aug 2015.

[21] M. Ivanovici and N. Richard, "Fractal dimension of color fractal images," *IEEE Transactions on Image Processing*, vol. 20, no. 1, pp. 227–235, Jan 2011.

[22] J. Yu, L. Tan, S. Zhou, L. Wang, and M. A. Siddique, "Image denoising algorithm based on entropy and adaptive fractional order calculus operator," *IEEE Access*, vol. 5, pp. 12 275–12 285, 2017.

[23] I. Zachevsky and Y. Y. J. Zeevi, "Statistics of natural stochastic textures and their application in image denoising," *IEEE Transactions on Image Processing*, vol. 25, no. 5, pp. 2130–2145, May 2016.

[24] I. Zachevsky and Y. Y. Zeevi, "Single-image superresolution of natural stochastic textures based on fractional brownian motion," *IEEE Transactions on Image Processing*, vol. 23, no. 5, pp. 2096–2108, May 2014.

[25] M. L. Uss, B. Vozel, V. V. Lukin, and K. Chehdi, "Efficient rotation-scaling-translation parameter estimation based on the fractal image model," *IEEE Transactions on Geoscience and Remote Sensing*, vol. 54, no. 1, pp. 197–212, Jan 2016.

[26] S. Khan and R. Guida, "On fractional moments of multilook polarimetric whitening filter for polarimetric sar data," *IEEE Transactions on Geoscience and Remote Sensing*, vol. 52, no. 6, pp. 3502–3512, June 2014.

[27] C. B. Gao, J. L. Zhou, J. R. Hu, and F. N. Lang, "Edge detection of colour image based on quaternion fractional differential," *IET Image Processing*, vol. 5, no. 3, pp. 261–272, April 2011.

[28] D. Quan and Y. S. Ho, "Interpolation scheme using simple multi-directional filters for fractional-pel motion compensation," *IEEE Transactions on Consumer Electronics*, vol. 56, no. 4, pp. 2711–2718, November 2010.

[29] A. M. Atto, "Ondelettes et processus stochastiques," *Ed. Lavoisier - Hermes Science Publications*, 2017.

[30] G. Dattoli, P. Ricci, and H. Srivastava, "Two-index multidimensional gegenbauer polynomials and their integral representations," *Mathematical and Computer Modelling*,

vol. 37, no. 3, pp. 283 – 291, 2003. [Online]. Available: http://www.sciencedirect.com/science/article/pii/S0895717703000062

[31] A. Krizhevsky, I. Sutskever, and G. E. Hinton, "Imagenet classification with deep convolutional neural networks," in *Advances in Neural Information Processing Systems 25*, F. Pereira, C. J. C. Burges, L. Bottou, and K. Q. Weinberger, Eds. Curran Associates, Inc., 2012, pp. 1097–1105.

[32] J. Deng, W. Dong, R. Socher, L. J. Li, K. Li, and L. Fei-Fei, "Imagenet: A large-scale hierarchical image database," in *2009 IEEE Conference on Computer Vision and Pattern Recognition*, June 2009, pp. 248–255.

[33] P. Appell and J. K. de Fériet, "Fonctions hypergéomtriques et hypersphériques polynômes d'hermite," *Gauthier-Villars, Paris*, 1926.

[34] B. Bahr and C. G. Esseen, "Inequalities for the rth moment of a sum of random variables, $1 \leqslant r \leqslant 2$," *Ann. Math. Statist.*, vol. 36, pp. 299 – 303, 1965.

TABLE I

TEST CONFUSION MATRIX FROM A DIRECT LEARNING: AVERAGE RETRIEVAL PER TEXTURE CATEGORY AND AVERAGE INTER-CATEGORY CONFUSION (IN %). THE $\mathcal{D}^3$ DATABASE IS COMPOSED BY 3 GFBF CATEGORIES (1800 TEXTURES FOR TRAINING, 1800 FOR LEARNING). THE $\mathcal{D}^4$ DATABASE IS COMPOSED BY 4 GFBF CATEGORIES (2400 TEXTURES FOR TRAINING, 2400 FOR LEARNING). THE CNN USED IS DESCRIBED IN APPENDIX C.

Test on $\mathcal{D}^3$			
X	1-GFBF	2-GFBF	3-GFBF
1-GFBF	94.50	3.83	1.67
2-GFBF	89.17	8.33	2.50
3-GFBF	85.00	10.50	4.50
Mean accuracy	35.78		

Test on $\mathcal{D}^4$				
X	1-GFBF	2-GFBF	3-GFBF	4-GFBF
1-GFBF	94.83	0	0.17	5.00
2-GFBF	89.33	0	1.33	9.33
3-GFBF	84.50	0	1.83	13.67
4-GFBF	84.83	0	2.00	13.17
Mean accuracy	27.46			

TABLE II

INDIRECT LEARNING (PSD FEATURE EXTRACTION PRIOR TO DEEP LEARNING STAGE): THE CONFUSION MATRIX (AVERAGE RETRIEVAL PER TEXTURE CLASS AND AVERAGE INTER-CLASS CONFUSION, IN %) SHOWS RELEVANT PERFORMANCE. THE $\mathcal{D}^3$ DATABASE IS COMPOSED BY 3 GFBF CATEGORIES (1800 TEXTURES FOR TRAINING, 1800 FOR LEARNING). THE $\mathcal{D}^4$ DATABASE IS COMPOSED BY 4 GFBF CATEGORIES (2400 TEXTURES FOR TRAINING, 2400 FOR LEARNING).

Test on $\mathcal{D}^3$			
X	1-GFBF	2-GFBF	3-GFBF
1-GFBF	100.00	0.00	0.00
2-GFBF	2.08	84.59	13.33
3-GFBF	0.00	16.67	83.33
Mean accuracy	89.31		

Test on $\mathcal{D}^4$				
X	1-GFBF	2-GFBF	3-GFBF	4-GFBF
1-GFBF	98.75	1.25	0.00	0.00
2-GFBF	2.50	77.92	19.16	0.42
3-GFBF	0.00	7.92	67.92	24.16
4-GFBF	0.00	6.25	32.08	61.67
Mean accuracy	76.56			

TABLE III

RECTIFIED LINEAR UNIT (RELU), ARCHITECTURE: CNN, TYPE ALEXNET / FULL TRAINING

# of Layer	Content	#N of Elements	Element size $n \times n$	# of Channels
1	'Fractional Images'	4800	448×448	1
2	'Convolution'	96	16×16	1
3	'ReLU'	Element-wise (one to one)		
4	'Normalization'	Cross channel with 5 channels/element and $(\alpha = 1, \beta = 0.75, \kappa = 1)$		
5	'Max Pooling'	Sub-sampling: maximum over a 3×3 spatial neighborhood		
6	'Convolution'	128	9×9	96
7	'ReLU'	Element-wise (one to one)		
8	'Normalization'	Cross channel with 5 channels/element and $(\alpha = 1, \beta = 0.75, \kappa = 1)$		
9	'Max Pooling'	Sub-sampling: maximum over a 3×3 spatial neighborhood		
10	'Convolution'	384	7×7	128
11	'ReLU'	Element-wise (one to one)		
12	'Convolution'	192	5×5	384
13	'ReLU'	Element-wise (one to one)		
14	'Convolution'	128	3×3	192
15	'ReLU'	Element-wise (one to one)		
16	'Max Pooling'	Sub-sampling: maximum over a 3×3 spatial neighborhood		
17	'Fully Connected'	Neuron matrix [Input size 8192 / Output size 16]		
18	'ReLU'	Element-wise (one to one)		
19	'Fully Connected'	Neuron matrix [Input size 16 / Output size 4]		
20	'Softmax'	Probability distribution with respect to 4 outputs		
21	'Classification'	Cross-entropy loss function with 4 categories as output		